FraMCos-9 Workshop in Honor of Zdeňek P Bažant

Cohesive crack analysis of concrete fracture

Luigi Cedolin

Department of Civil and Environmental Engineering

Politecnico di Milano – Milan Italy

Outline

- Experimental investigations on **tensile** behavior of concrete
- Hilerborg’s Fictitious Crack Model
- Bažant’s Crack Band Model
- Identification of the Cohesive Crack softening law from wide field measurements of tensile deformations
- Relation between Hillerborg’s Cohesive Crack Model and Bažant’s Size Effect Law

Tensile Tests on Unotched Specimens

The tensile failure of concrete (which initially was interpreted as a sudden rupture of the material) was explained in the sixties, when researchers became aware of the existence of a softening branch of the load-displacement curve if tests were performed under displacement control.

In the next slides, some meaningful contributions of those years are presented in the format of σ–w relations, proposed by D.A. Hordijk (1989, TU Delft) in his Survey of Deformation-Controlled Tests.

Rusch and Hildorf (1963)

Total relative displacement ***Δ*** across gage length

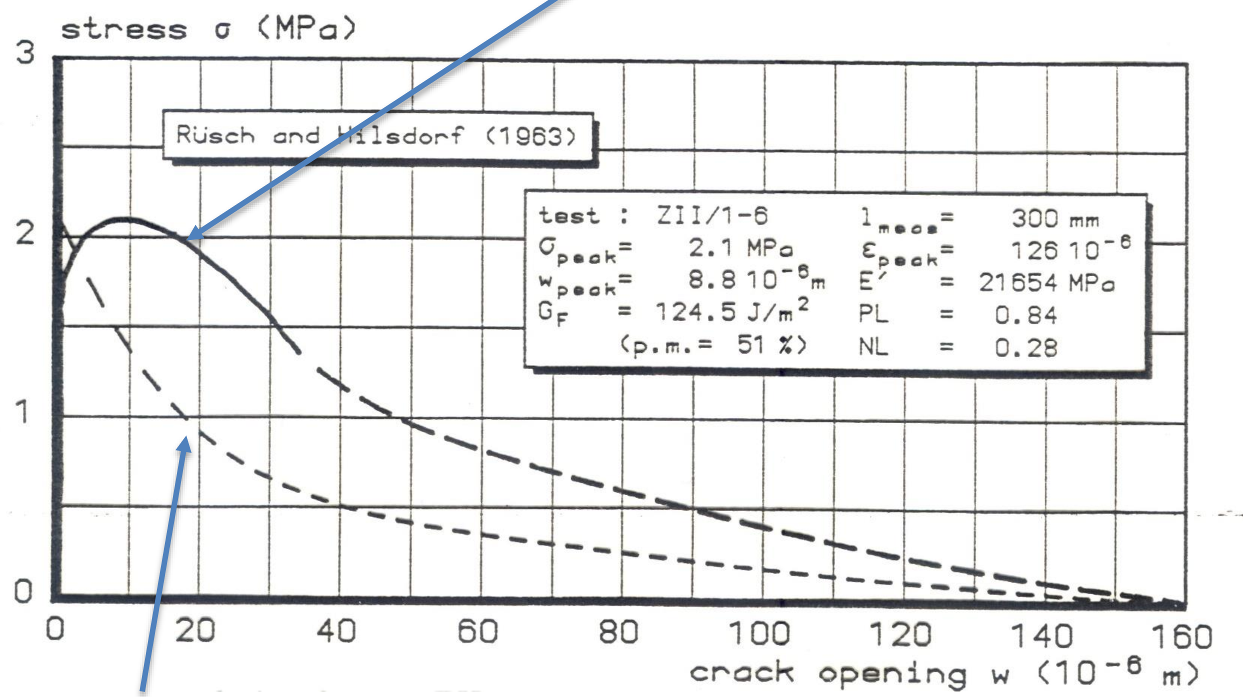

Crack opening displacement ***w***, calculated by subtracting from ***Δ*** the elastic displacement

Hughes and Chapman (1966)

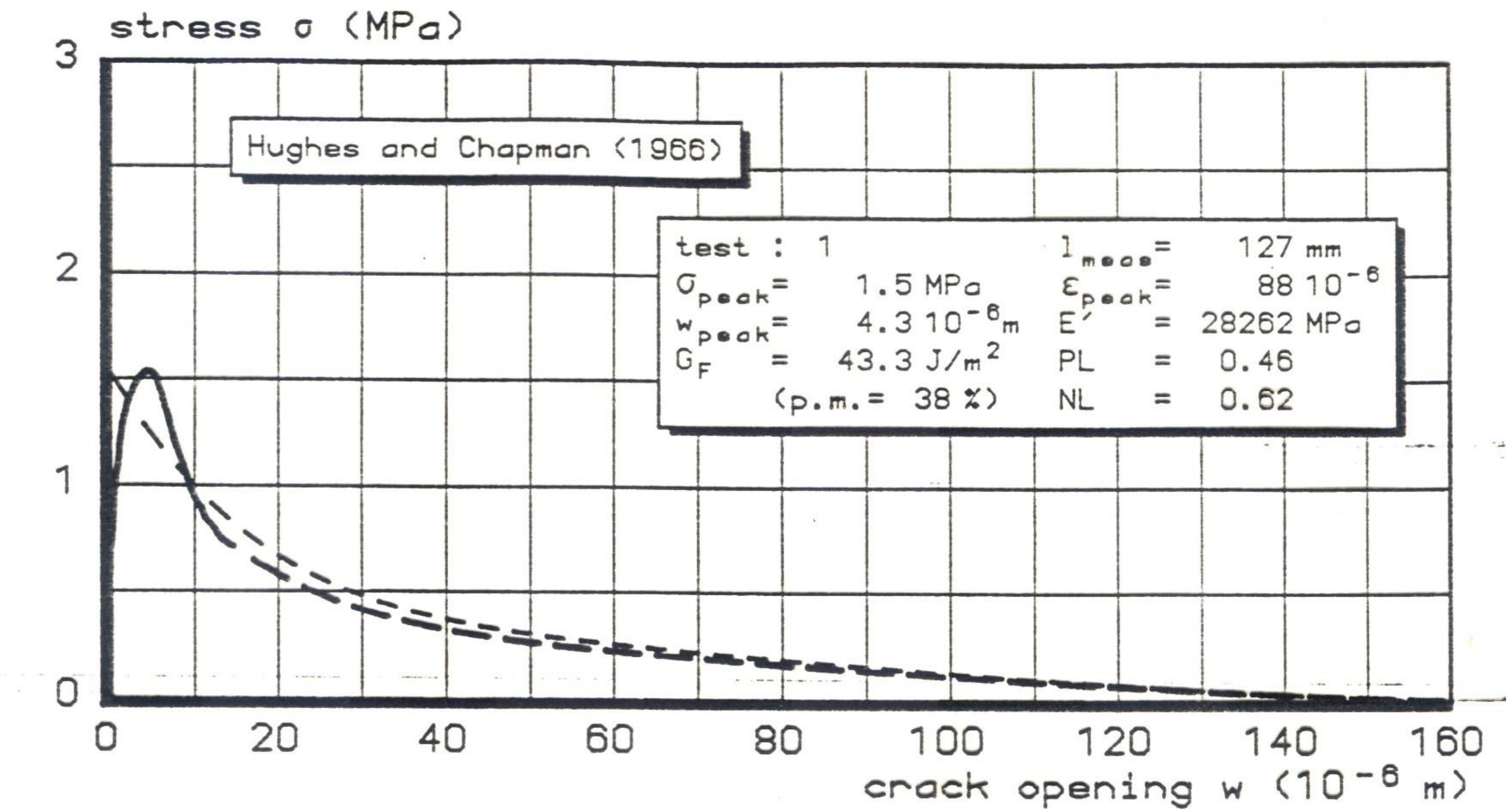

Evans and Marathe (1968)

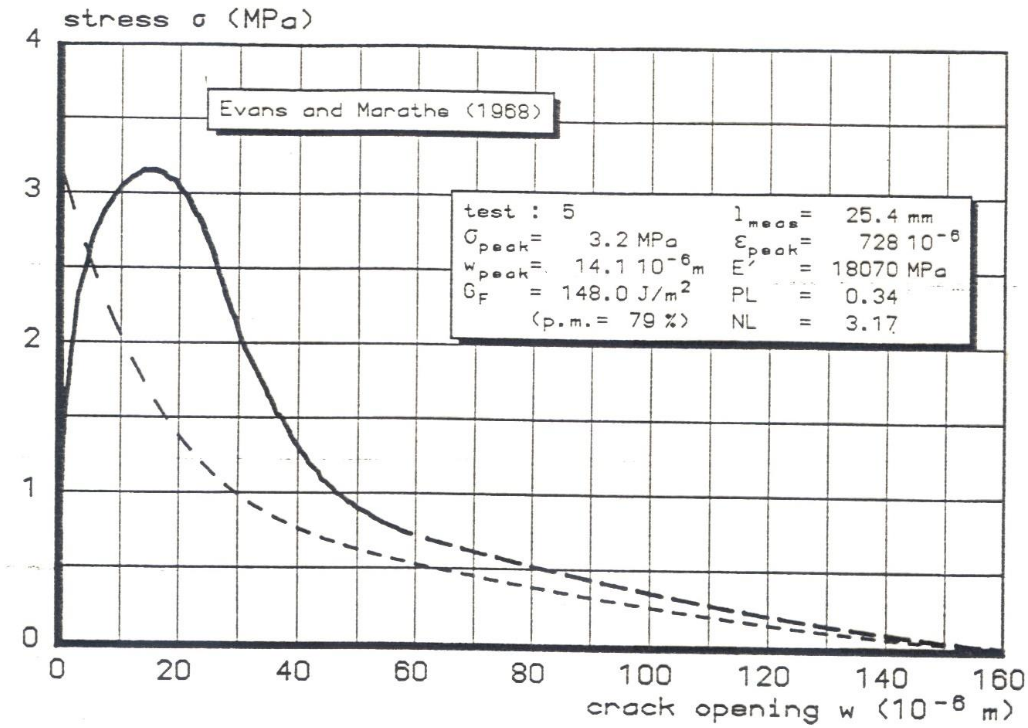

Hordijck notes that probably Evans and Marathe were first in recognizing that: «The large strain values observed in these tests are primarily due to the ***initiation of a microcrack*** *between the gage length (25-60mm)»*

Heilmann Hilsdorf Rusch (1969)

Along the central part of the specimen, a series of electrical extensometers of 60 mm length were attached to the specimen in order to capture the strain localization

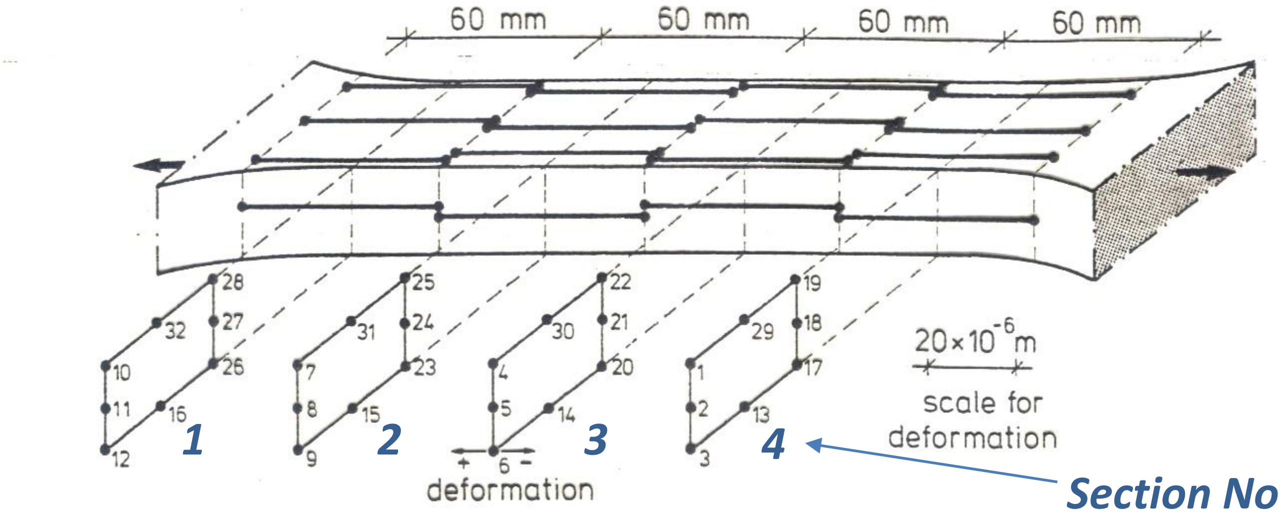

In the next slide we will see an example in which the strain localized in Section 1

Heilmann Hilsdorf Rusch (1969)

Strain distribution in the four Sections during loading history up to total crack propagation

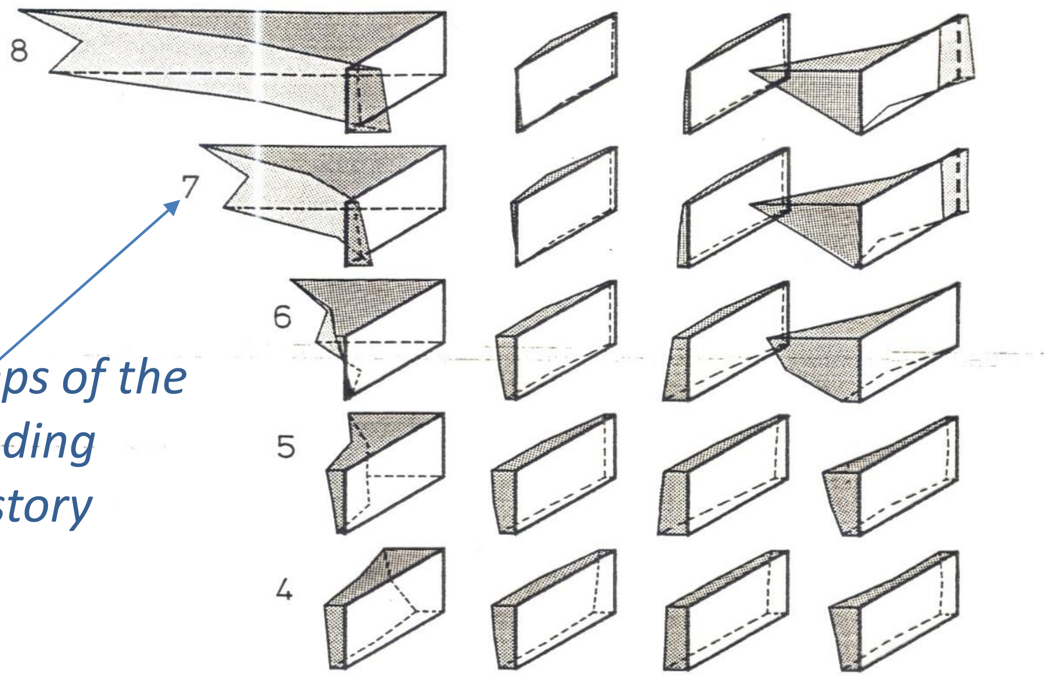

Steps of the loading hystory

*The strain localizes **non-uniformly** in the 60 mm length represented by Section 1*

Tests on Notched Specimens

Tests conducted in the same period on notched specimens were showing contradictory results regarding the application of LEFM .

The first results were published by **Kaplan (1961)**, who found that the values of $\mathbf{G_f}$ for the same concrete were not constant for different types and sizes of specimens.

Walsh (1972) recognized that one cause of this variabilty was the size of the specimens, and showed that for larger specimens the predictions of linear fracture mechanics were valid, while smaller specimens appeared to be notch-insensitive.

Kesler, Naus and Lott (1972), recognized the existence, in the proximity of the notch, of very high local strains attributable to microcracked material, and concluded that linear fracture mechanics was not applicale to concrete.

Numerous other investigations detected a **stable crack growth**, which indicates the need of nonlinear fracture mechanics.

Hillerborg's Fictitious Crack Model

The so far elusive experimental findings of tensile tests on both notched and unnotched specimens were modeled by **Hillerborg, Modeer** and **Petersson** (1976) through the use of a ***softening relation*** between the **stress *σ* transmitted across the crack** and the **crack opening displacement *w*.** This softening relation represents the **progressive rupture of bonds** across the crack surfaces, so that the **area under the softening curve** represents the **fracture enegy G_f .**

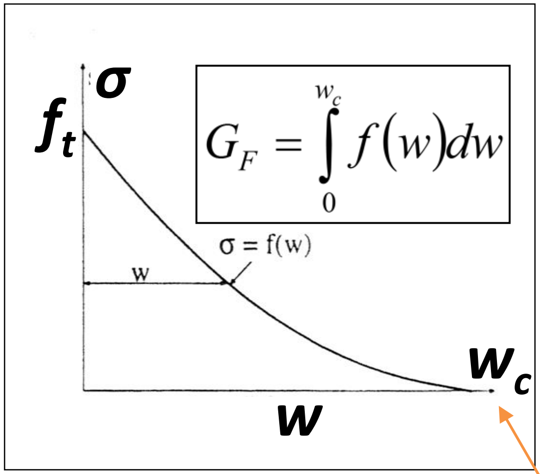

Three parameters:
- *Peak stress* f_t
- *Critical crack opening* w_c
- *Form of the softening curve*

Fracture simulations

Hillerborg, Modeer and Petersson characterized the energy consumption capacity of the material in the fracture process zone through the ***characteristic length*** $l_{ch} = G_f E/f_t^2$.

With reference to a **linear-type softening law** and using an **inter-element discrete crack** representation, they proved that the model would give appropriate predictions of the flexural strength of **un-notched** concrete beams. The model, denominated «**Fictitious Crack Model**» (**Modeer**, 1979), was also applied to the simulation of fracture of several types of notched specimens (**Peterson**, 1981), showing its predictive capabilities.

Bažant's Crack Band Model

In the meantime it had become possible to perform numerical analysis of **reinforced** concrete members with the **Finite Element Method**, using **Rashid**'s (1972) **smeared** crack concept and a **strength** criterion for **crack propagation.** **Bažant and Cedolin** (1976) proved that this criterion would lead to results which depended heavily on the size of the elements in the adopted mesh. They also proved that an energy criterion for smeared crack propagation was capable of simulating fracture problems with no need for singularity elements.

For **plain** concrete, however, the smeared crack simulation of the results of **fracture tests** was not successful until **Bažant** (1981) introduced the concept of a **crack band** of **distributed microcracks, characterized** by a **softening** stress-**strain** relation and by an **effective** value $h_c = 2\alpha E G_f / f_t^2$ ($\alpha = (1 - E/E_t)^2$) of its width. This model satisfies the theoretical requirement (**Bažant** and **Belytschko, 1985**) that a softening continuum must be accompanied by a localization limiter.

Crack Band Simulations

Bažant and **Ho (**1983) used the crack band model (which has a much greater flexibilty than the discrete crack approach) to simulate the fracture tests reported in the literature. They fitted the peak load data assuming G_f, f_t and h_c as independent material parameters for each concrete, and found that the assumption of a constant value for the ratio **crack band width/ aggregate size = 3** would not change the accuracy of the predictions.

They also performed a very rigorous statistical analysis of the results, showing that the material model would fit very well **various geometries**, **sizes** and **loading conditions**, and this furnished a definitive proof of the predictive capability of the softening relation for the **fracture process zone** .

Experimental Determination of Deformation Field

The success of a **softening relation** in explaining the **peak-load** test results on notched specimens was a further stimulus to find an **alternative method** for its **experimental determination**, being the **direct tensile test** undermined by the **non-uniform distribution** of strains (and stresses) in the cross-section.

This problem could be overcome (as proposed by **Cedolin**, **Dei Poli** and **Iori**,1981) by measuring the **deformation field** in the entire region affected by the crack propagation, using **laser moiré interferometry**. With this technique, a laser beam is split into two rays which by interference generate a **virtual reference grid** (oriented transversally) of **1000** lines/mm. This grid is also **engraved** on the specimen's surface and deforms with it. The interference of the two grids (virtual and real) generates a **pattern of moiré fringes**, from which it is possible to determine both the **longitudinal strain** in the **microcracked zone** and the **crack opening profile**.

Measurement Apparatus

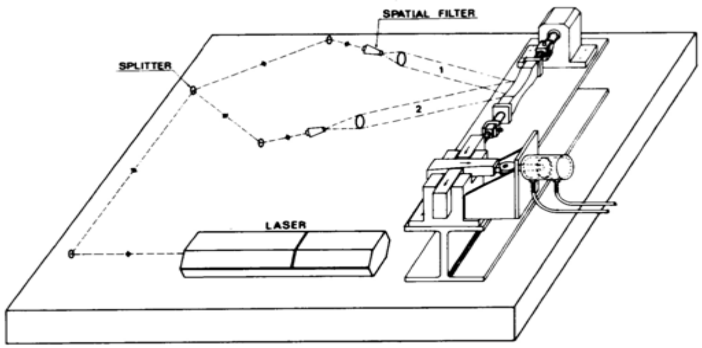

Vibration Insulated marble plate

Loading Device

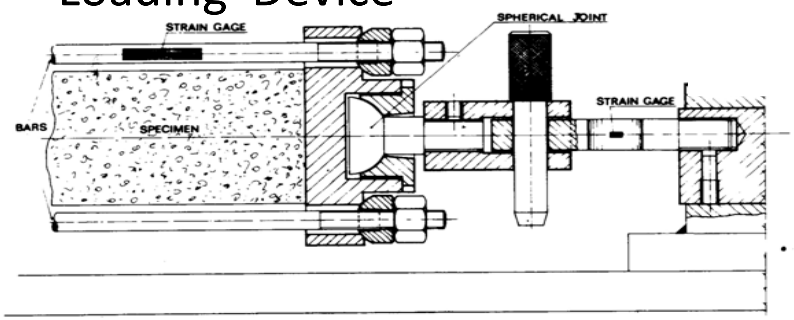

Grid engraved on layer
of photoresist

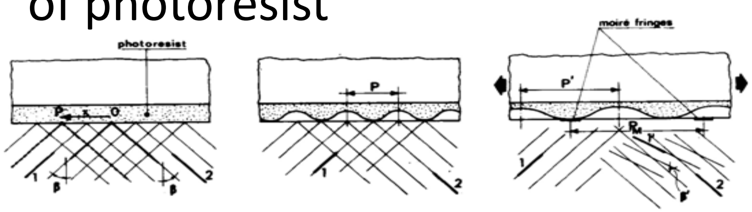

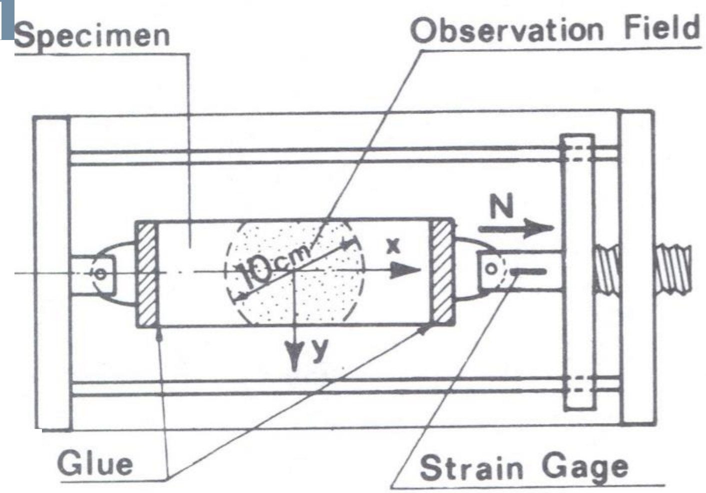

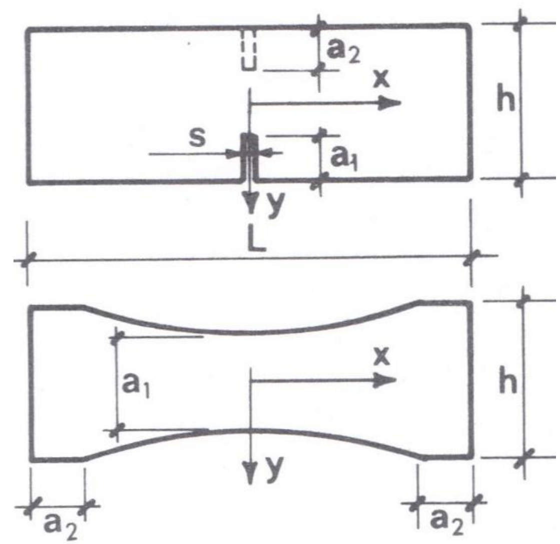

Tensile Test on Un-notched Specimen

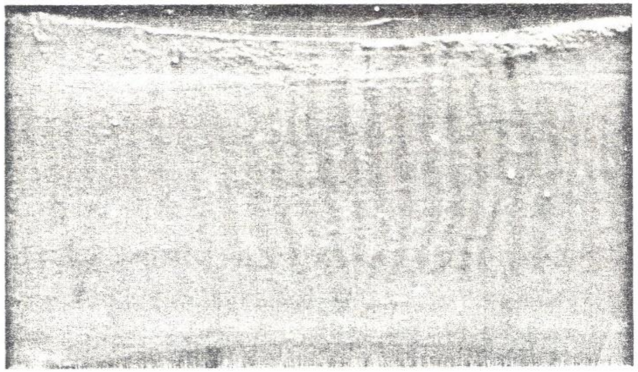

Specimen D0-1

Fringe pattern

Contour of micro-cracked zone

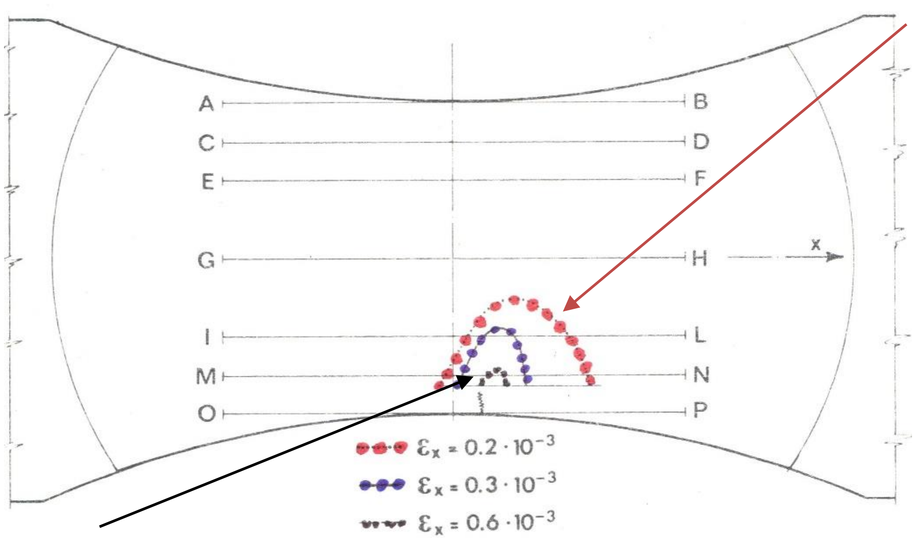

Discrete crack

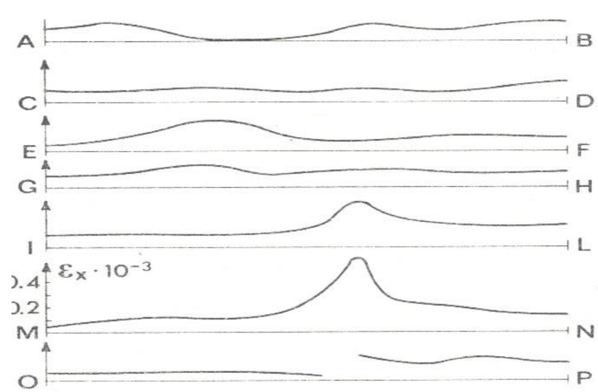

Longitudinal strain distributions

Subsequent crack propagation stages

Specimen D0-3

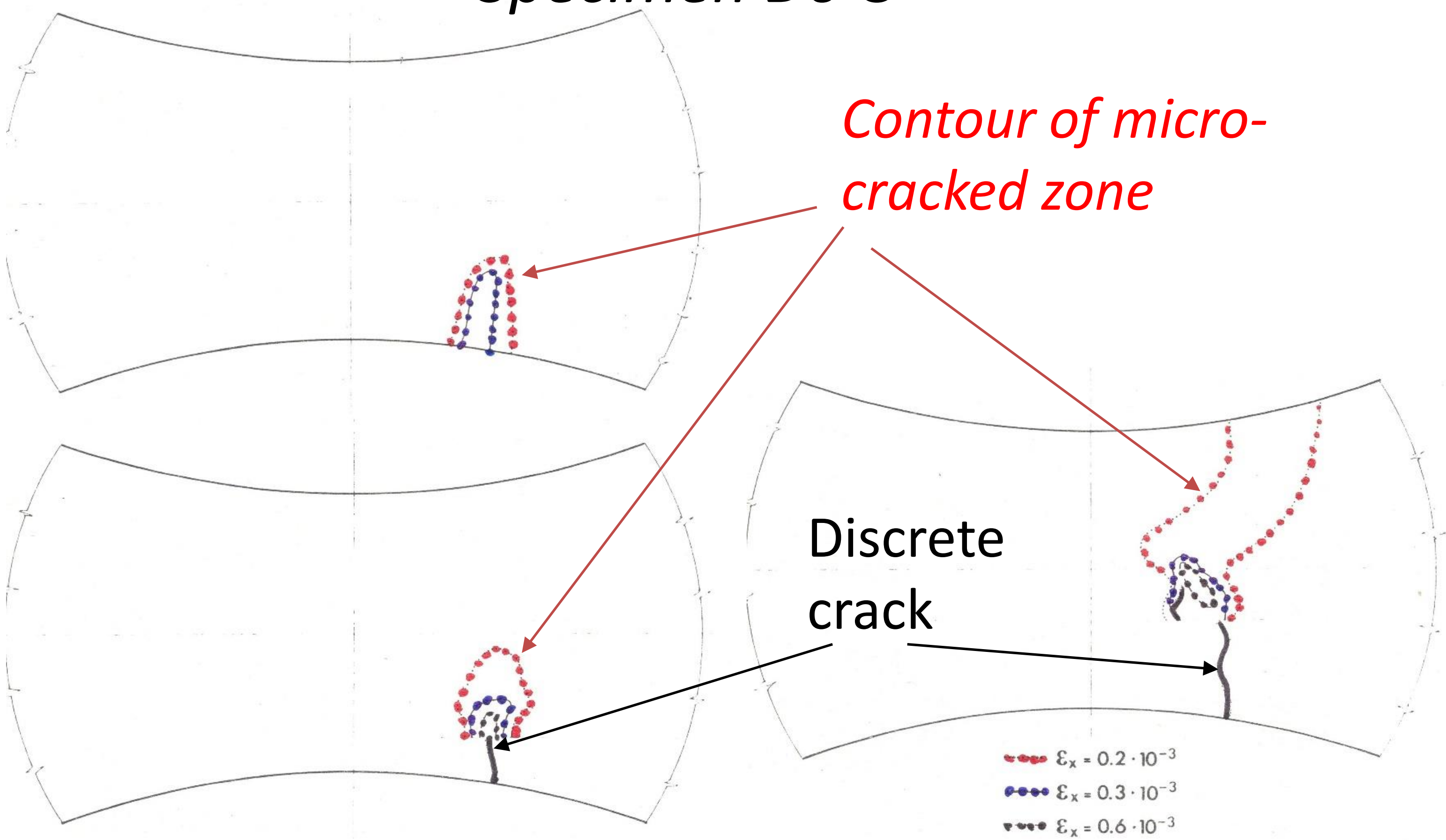

Virtual extensometers strain measures

Specimen D0-7

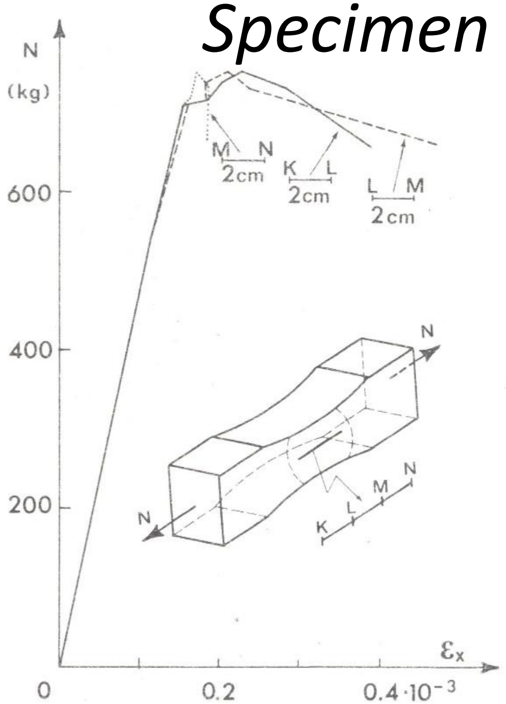

Extensometers
differently
located

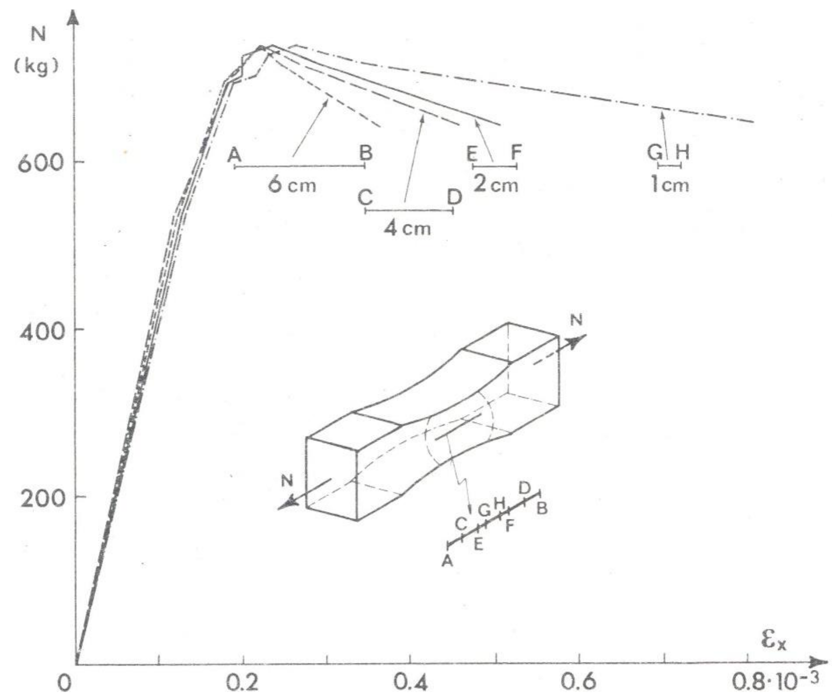

Extensometers
of different
length

Fracture Process Zone

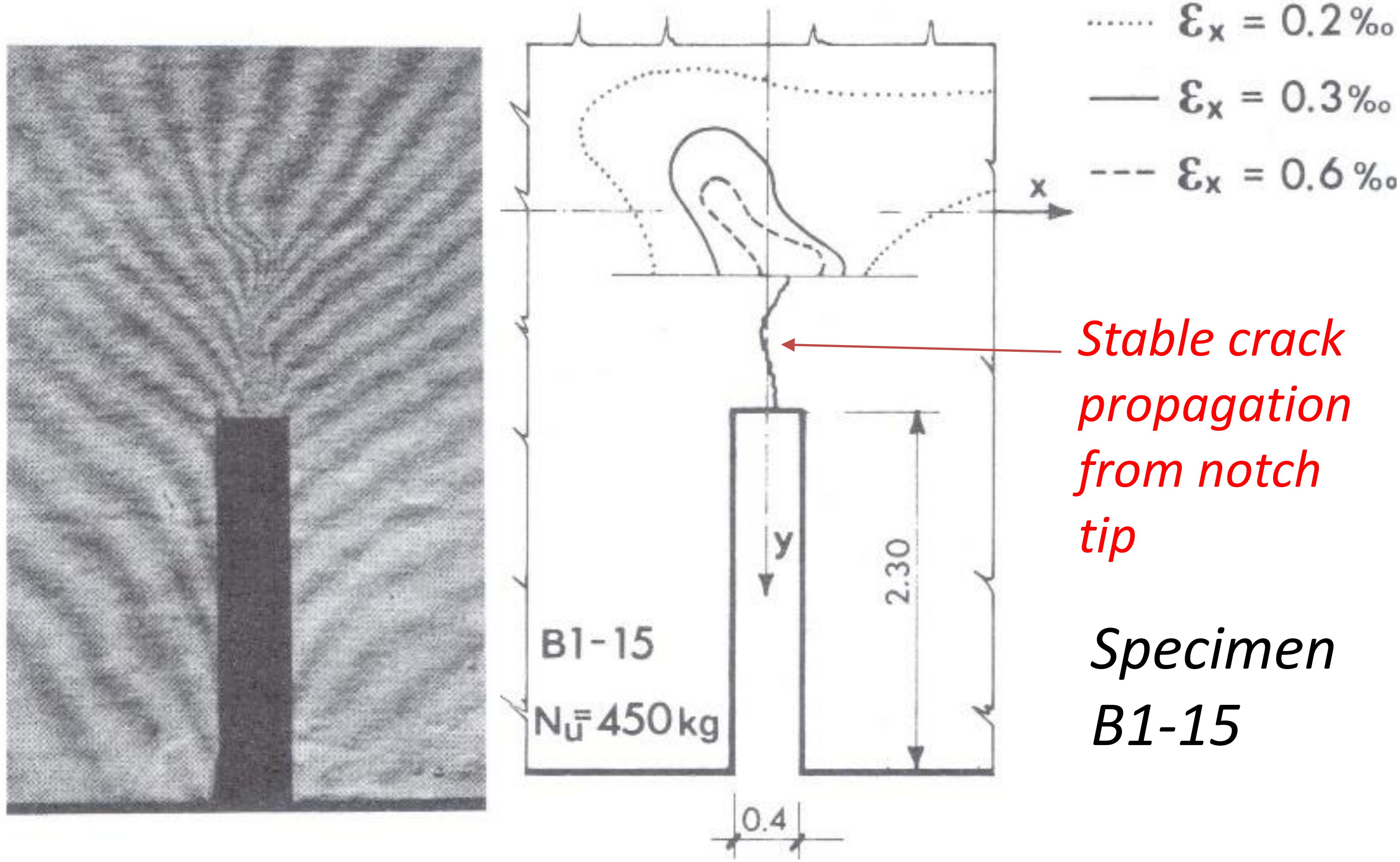

Stable crack propagation from notch tip

Specimen B1-15

FPZ Propagation

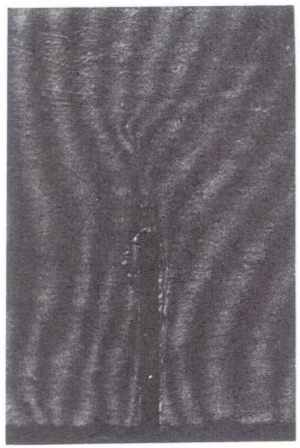

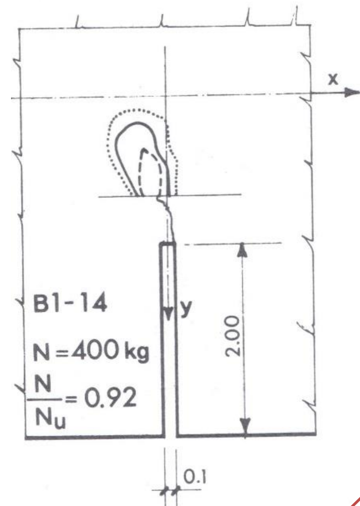

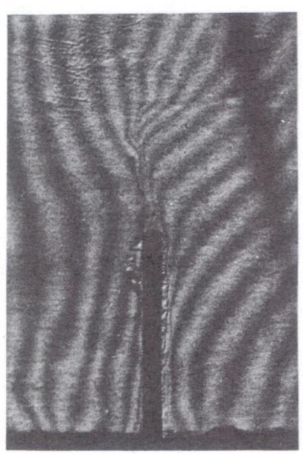

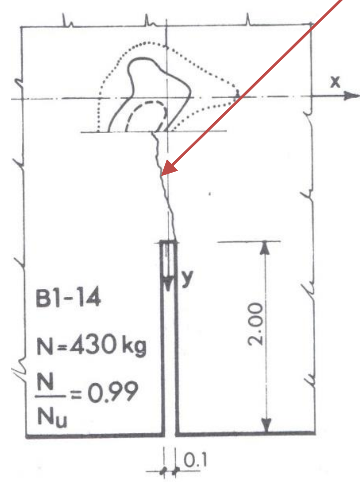

$\cdots\cdots$ ε_x = 0.2 ‰

—— ε_x = 0.3 ‰

- - - ε_x = 0.6 ‰

Specimen B1-14

Crack propagation before failure

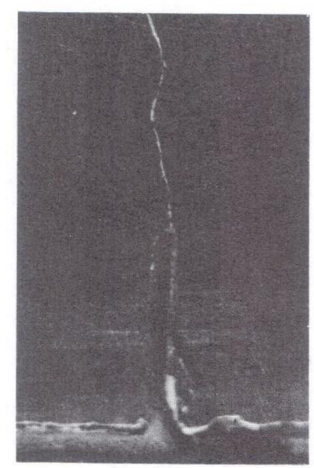

Image of actual crack

Deformation Field

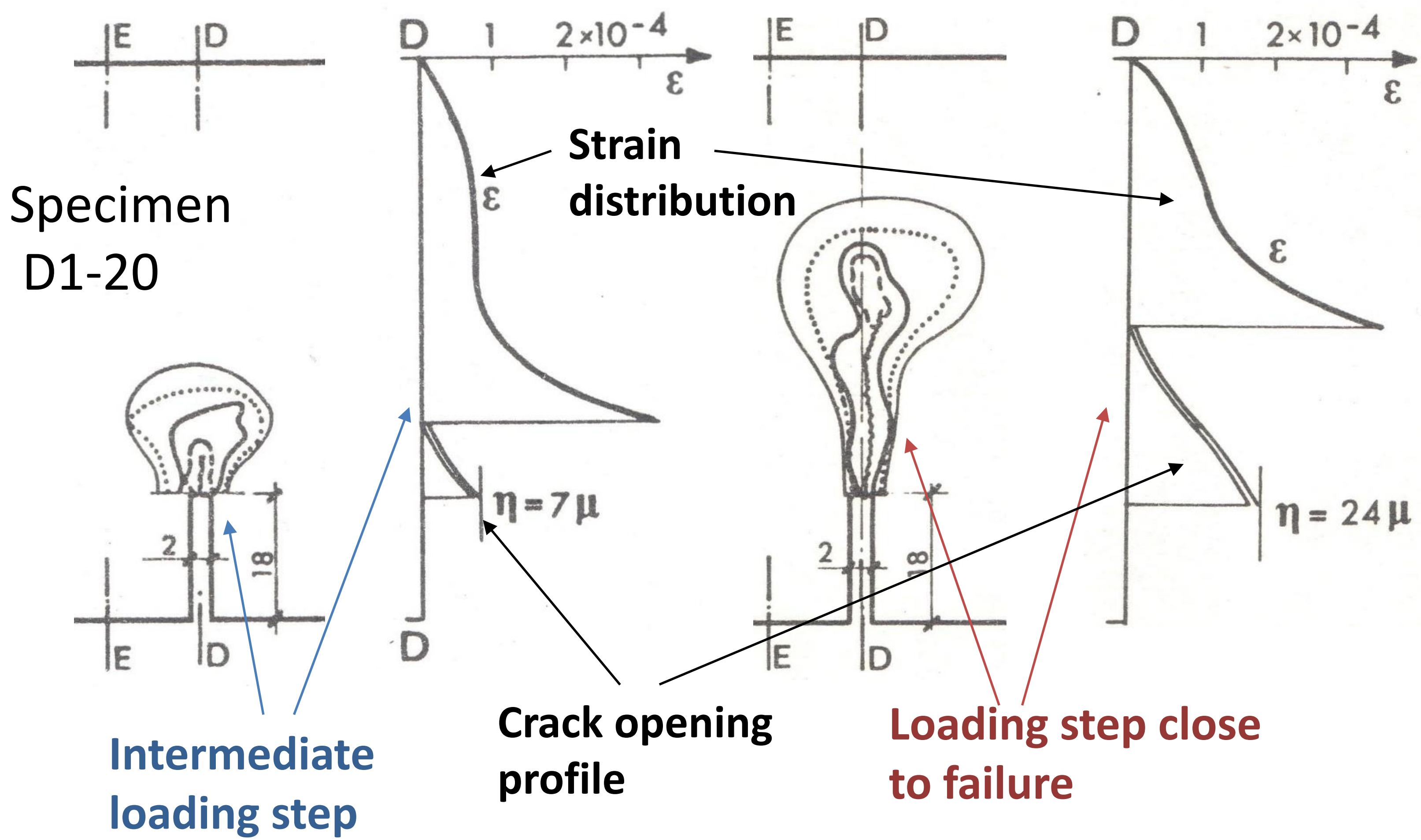

Measured Deformation History

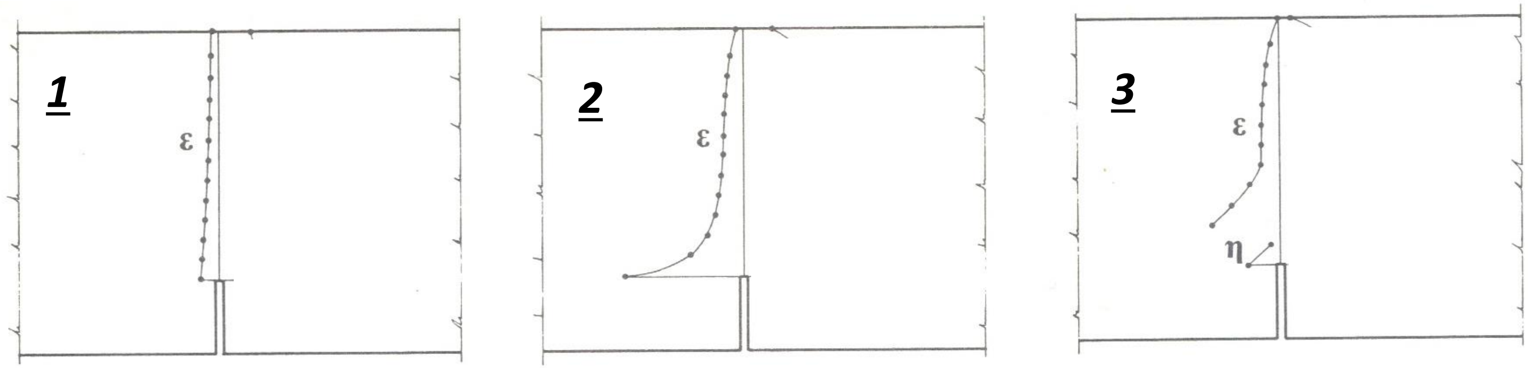

Specimen D1-20

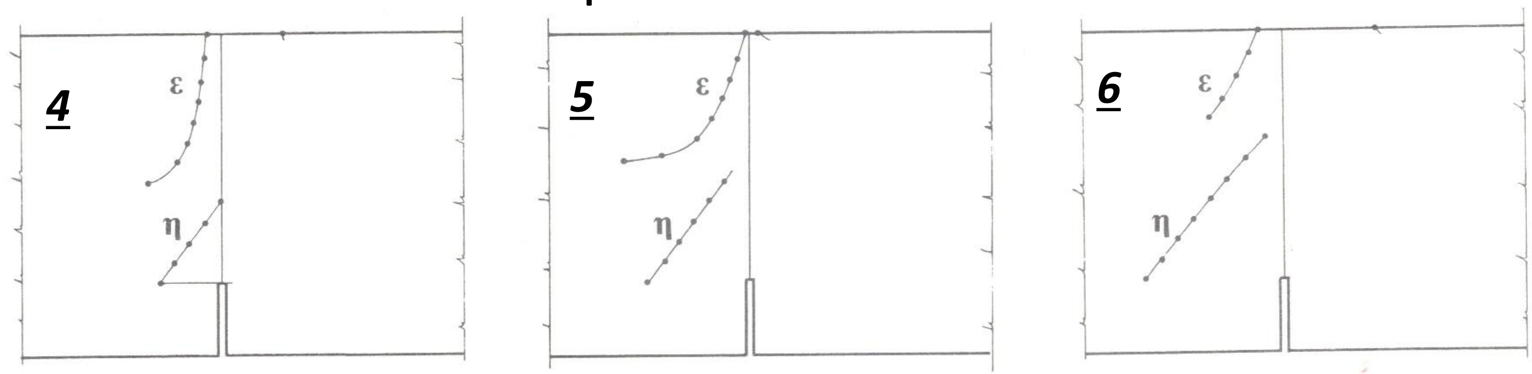

The **unknown stress** distributions correponding to the various **measured strain** and **crack opening** distributions may be identified by imposing the equilibrium with a **centered known** axial force (rotating loading platens).

Identification of Material Laws

Considering **7 loading steps** there were then **14 conditions of equilibrium** that were used to identify the **2 unknown** parameters ($\bar{\sigma}$ and $\bar{\eta}$ or η^*) of the expressions shown below for the **stress-strain** and **stress-opening displacement** relations ($\bar{\varepsilon}$ is an empirical constant). An optimization algorithm selected the **solid line** curves with respect to the other possible choices.

$$\sigma = \frac{E\epsilon}{1 + \left(\frac{E}{\bar{\sigma}} - \frac{1}{\bar{\epsilon}}\right)\epsilon}$$

$$\sigma = \bar{\sigma}\left(1 - \frac{\eta}{\bar{\eta}}\right)$$

$$\sigma = \bar{\sigma} e^{\eta/\eta^*}$$

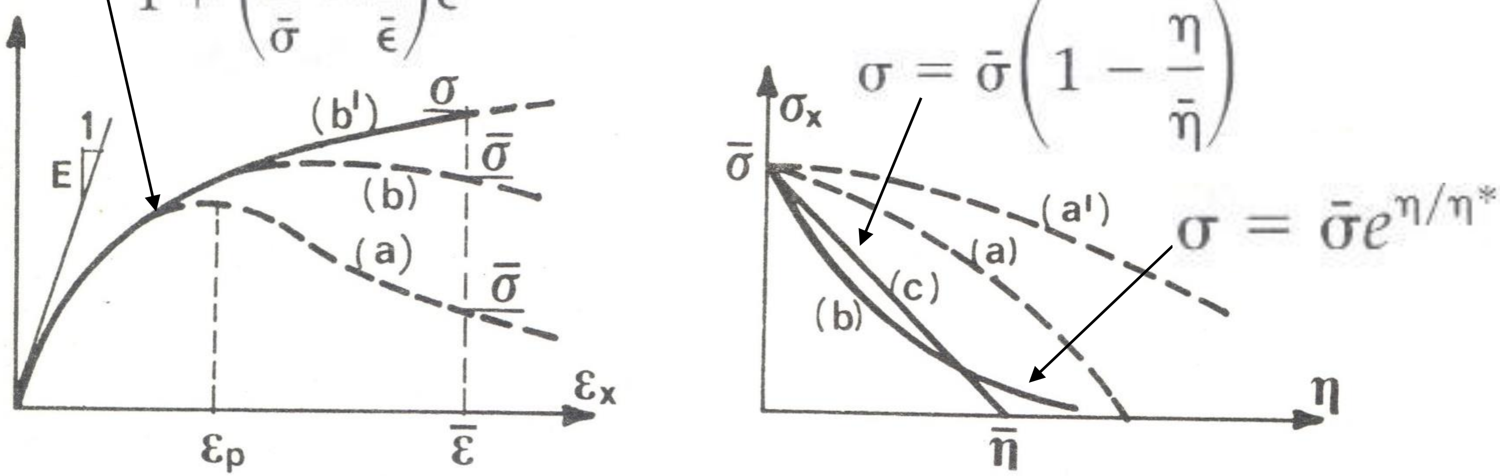

Stress History

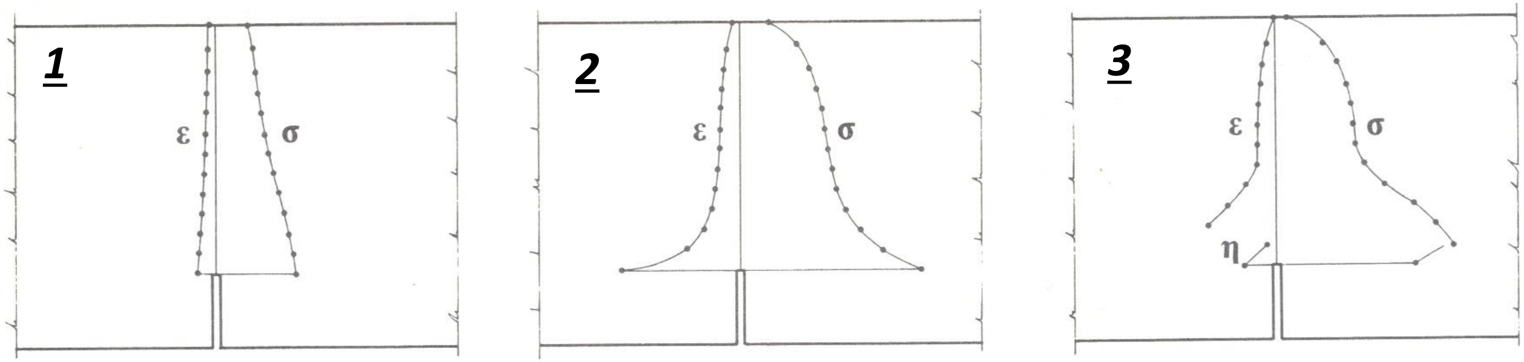

Specimen D1-20

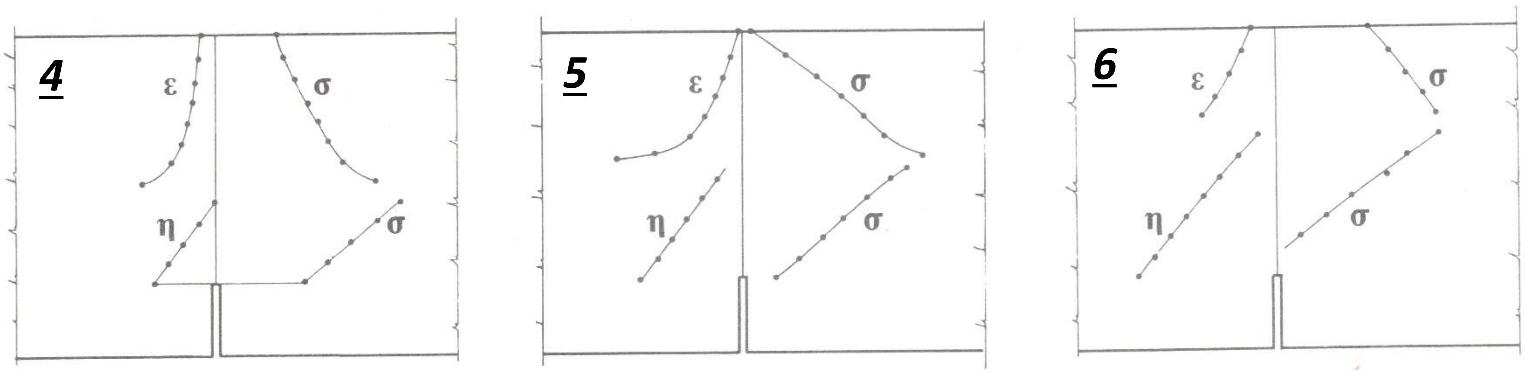

Distribution of stresses corresponding to the identified cohesive crack material laws.

Fracture Process Zone Analysis

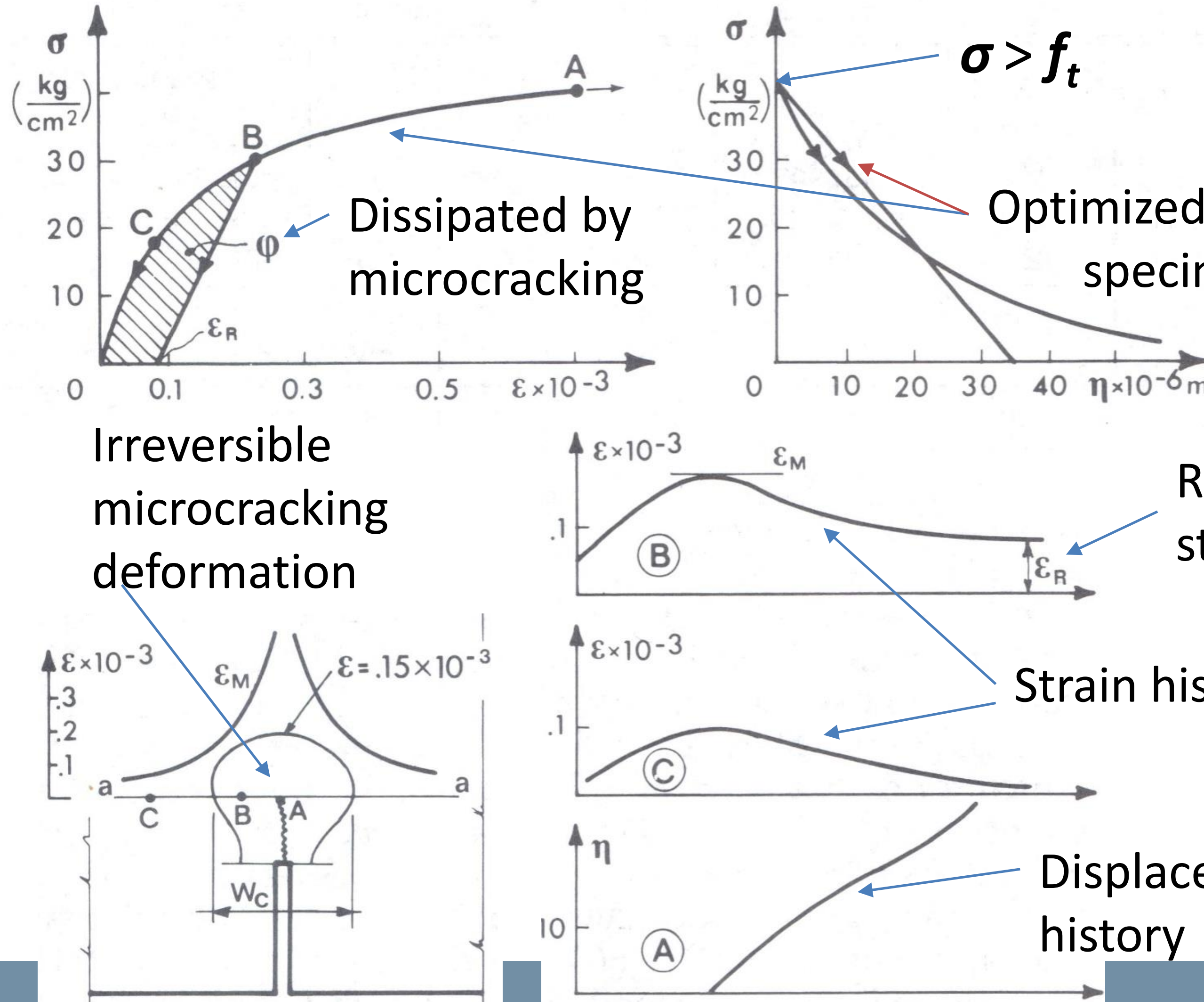

Components of Dissipated Energy

ε=1.5x10^{-3}

Specimen D1-20

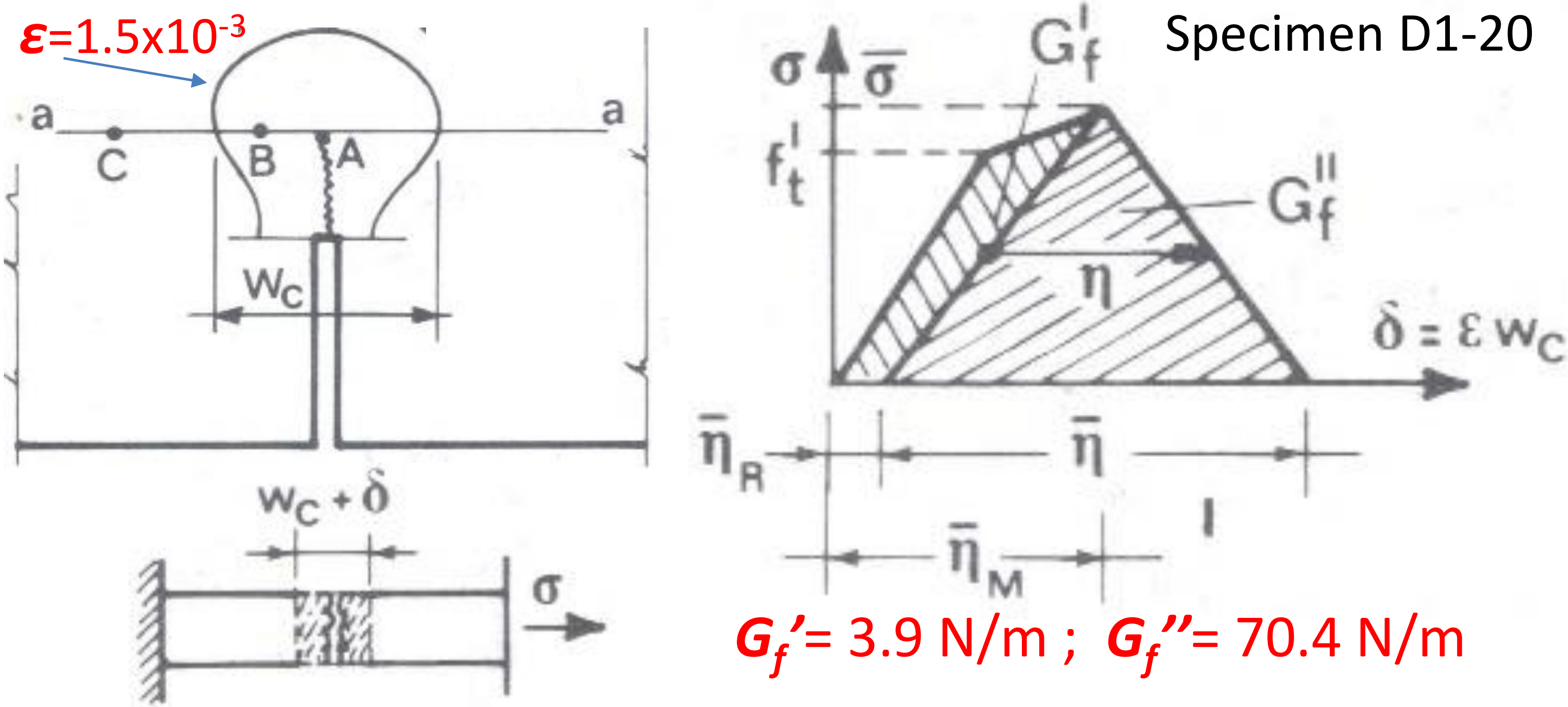

G_f'= 3.9 N/m ; G_f''= 70.4 N/m

The energy dissipated along the line **a-a** during the entire loading history can be separated in two contributions: G_f' diffused in the microcracked **bulk** material (for example point B); G_f'' concentrated on the discrete crack (point A) and **real fracture energy**.

Bažant's Size Effect Law

A way to take into account the presence of a *Fracture Process Zone* (FPZ) of not negligible size ahead of the crack tip was proposed by **Bažant** in 1984 by applying **LEFM** to an **"effective"** critical crack length $a_0 + c_f$, being c_f a crack extension.

Expressing the energy release rate as

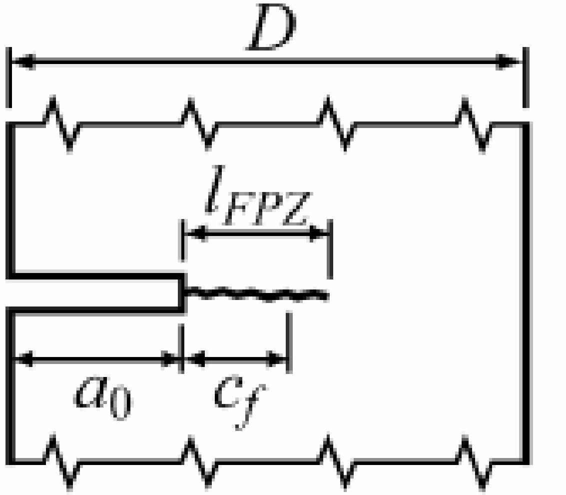

$$g(a_0 + c_f/D) \approx g(a_0) + g'(a_0)c_f/D$$

he obtained the ***Size Effect Law*** **(SEL)**

$$\frac{1}{\sigma_N^2} = \frac{g(a_0)}{E\,G_f} D + \frac{g'(a_0)\,c_f}{E\,G_f}$$

The fitting through **linear regression** of the experimental max nominal stresses $\boldsymbol{\sigma_N}$ of specimens of the same geometry but different sizes leads to the identification of $\boldsymbol{G_f}$ and $\boldsymbol{c_f}$.

Bažant's Size Effect Law *(SEL)*

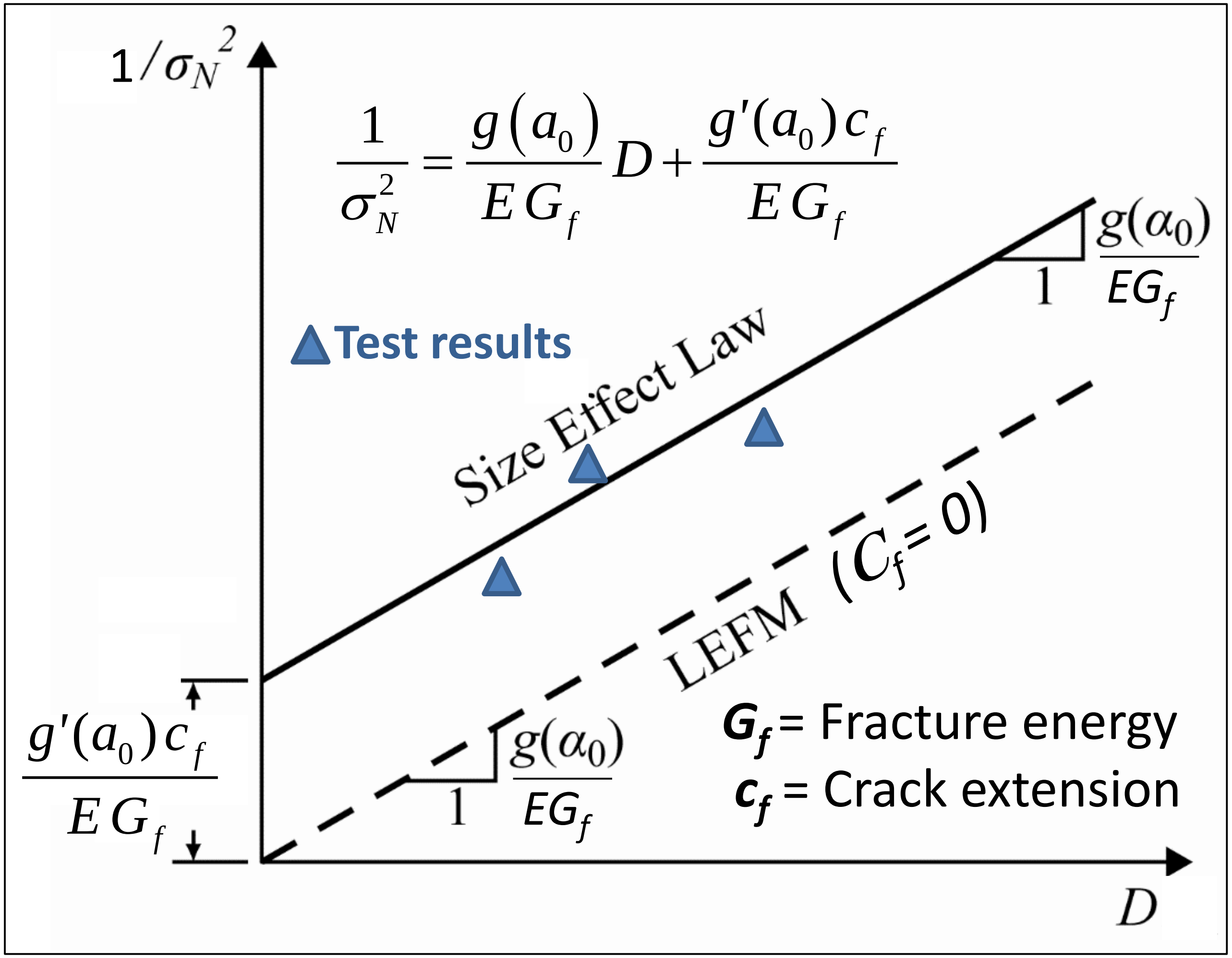

Cohesive Crack Simulations

The softening curve may be well represented by a bilinear law with an initial steep slope followed by a tail with mild inclination.

For specimens of **not large size**, only the initial part of the softening curve, characterized by the tensile strength $\boldsymbol{f_t}$ and the *initial* fracture energy $\boldsymbol{G_f}$ (area under the *initial tangent*), determines (**Planas,** 1992) the maximum nominal stress $\boldsymbol{\sigma_N}$.

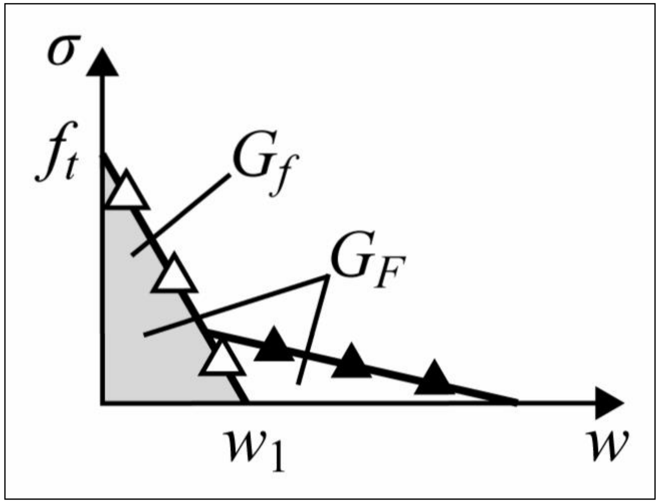

In this case by considering specimens of the **same geometry** but **different sizes** it is possible (**Planas**, 1997) to interpolate the results of FE simulations through an approximate relation which defines a **Cohesive Size Effect Curve (CSEC)**

$$\sigma_N = f_t \psi\left(\frac{D}{l_{ch}}\right) \qquad \left(\frac{f_t}{\sigma_N}\right)^2 = \Phi\left(\frac{D}{l_{ch}}\right) \qquad (l_{ch} = E\, G_f / f_t^2)$$

Relation with Bažant's Size Effect Law

- Recast SEL utilizing characteristic length

$$\left(\frac{f_t'}{\sigma_{Nu}}\right)^2 = g_0 \frac{D}{l_{ch}} + g_0' \frac{c_F}{l_{ch}}$$

- CSEC asymptote equivalent to SEL?

$$\left(\frac{f_t'}{\sigma_{Nu}}\right)^2 = \kappa_0 \frac{D}{l_{ch}} + \kappa_1$$

  - $\kappa_0 = g_0$
  - $\kappa_1 = g'_0 \, (c_F/l_{ch})$;

- If c_F is a material property:

$$\frac{c_F}{l_{ch}} = \frac{\kappa_1}{g_0'} = \quad \text{constant}$$

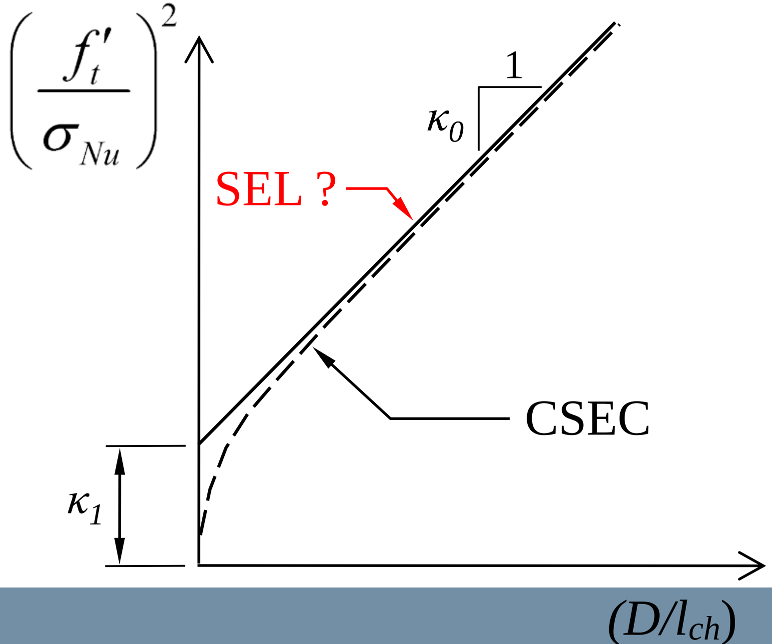

Numerical Calculation of Cohesive Size Effect Curve

The numerical simulations through FE were performed (Cedolin and Cusatis, 2008) with reference to **3 different specimen geometries,** using **zero-thickness interface elements** with a **linear** cohesive crack law.

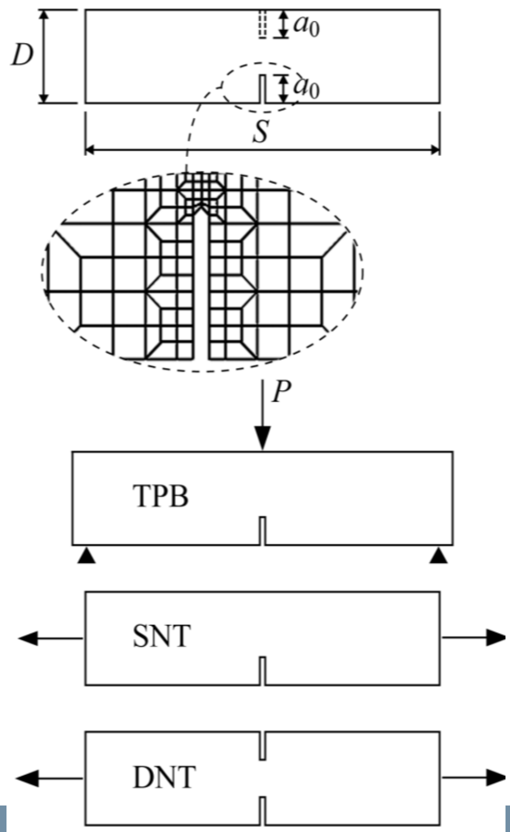

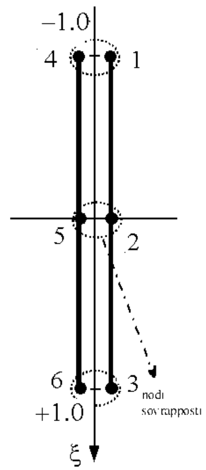

F.E. Meshes: they were designed with the aim of giving an accurate representation of the stress profile in the FPZ

Geometry : $\boldsymbol{D}$ **= 60** to **3840 mm** ;
$S/D = 4$; $a_0 = \alpha_0 D$; $\alpha_0 = 0.3$
notch width = 3 mm (constant)

Mechanical properties: $\nu = 0.2$
$E = 30000$ N/mm^2 ; $\boldsymbol{f_t = 3}$ **N/mm²**
$\boldsymbol{G_f = 0.030}$ **N/mm (linear softening)**
$\boldsymbol{l_{ch} = E\, G_f \,/\, f_t^2 = 100}$ **mm**

Three Point Bending Specimens

Nominal stress
$\sigma_N = 3P_{max}S/(2BD^2)$

Asymptote
$Y = AX+C$
$A = 1.021$; $C = 2.036$
$g(\alpha_0) = 1.025$ (Tada)

$$C = \frac{g'(\alpha_0)c_f}{l_{ch}}$$

$$c_f = \frac{CEG_f}{g'(\alpha_0)f_t^2} = 38.8\text{mm}$$

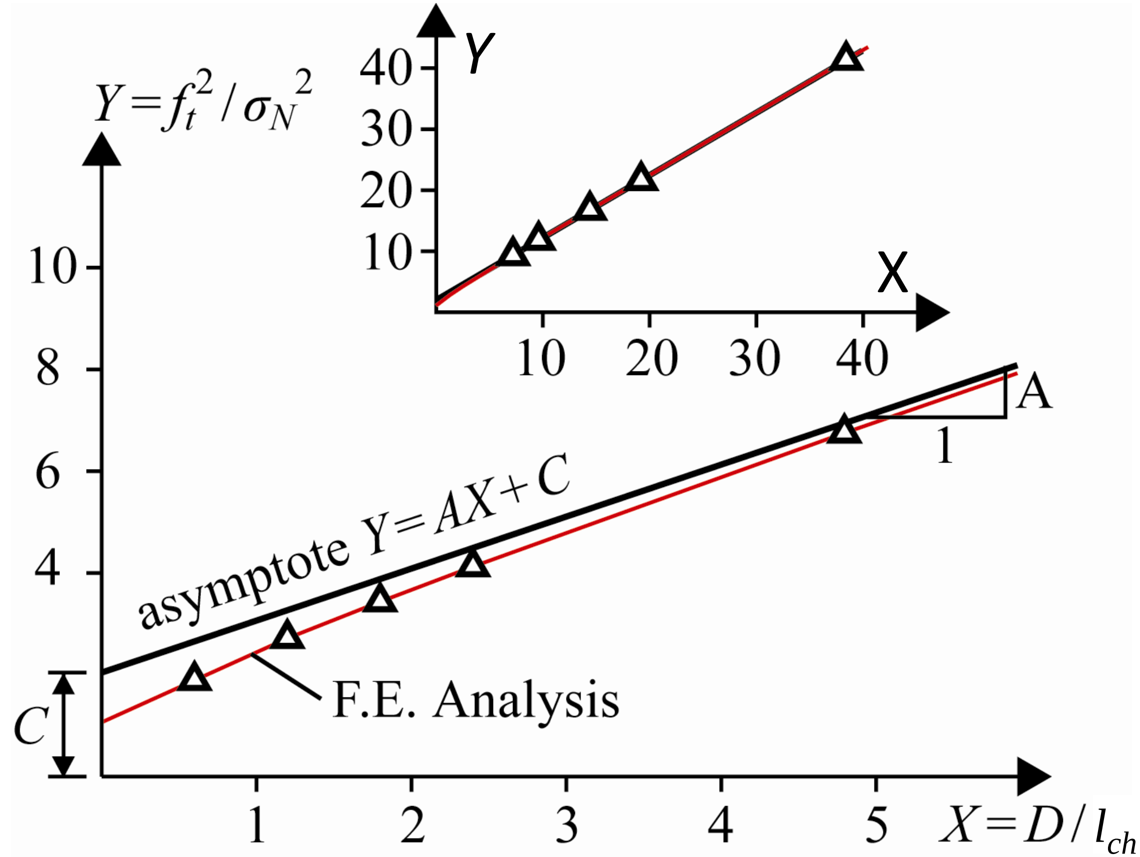

Fracture Process Zone

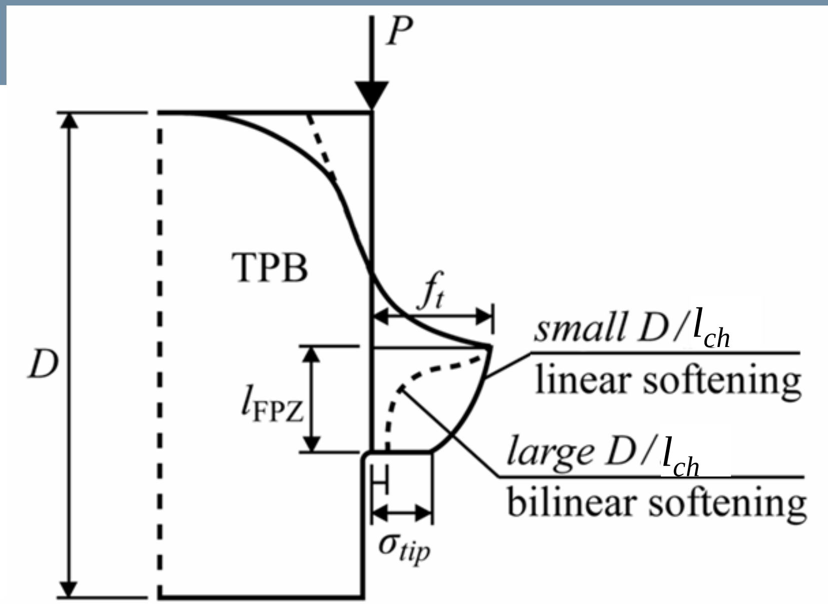

Numerical results
for TPB Specimens

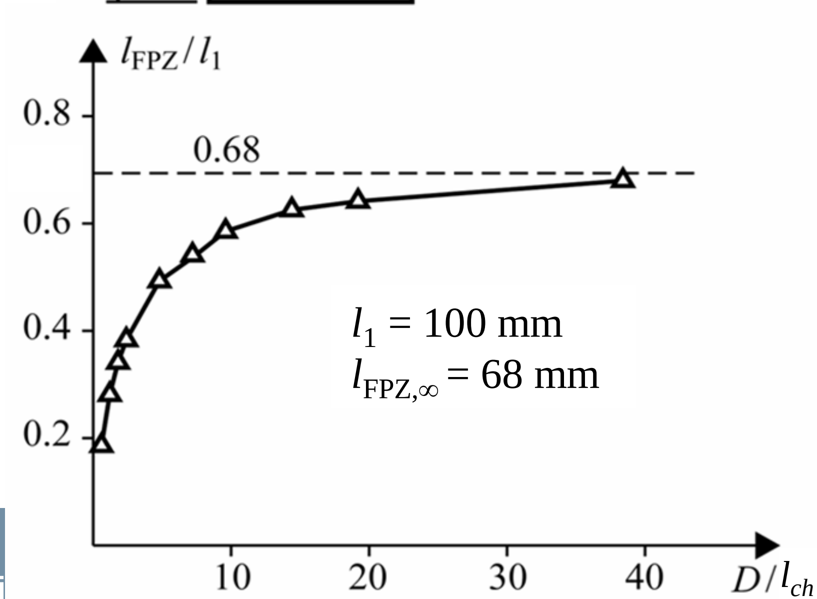

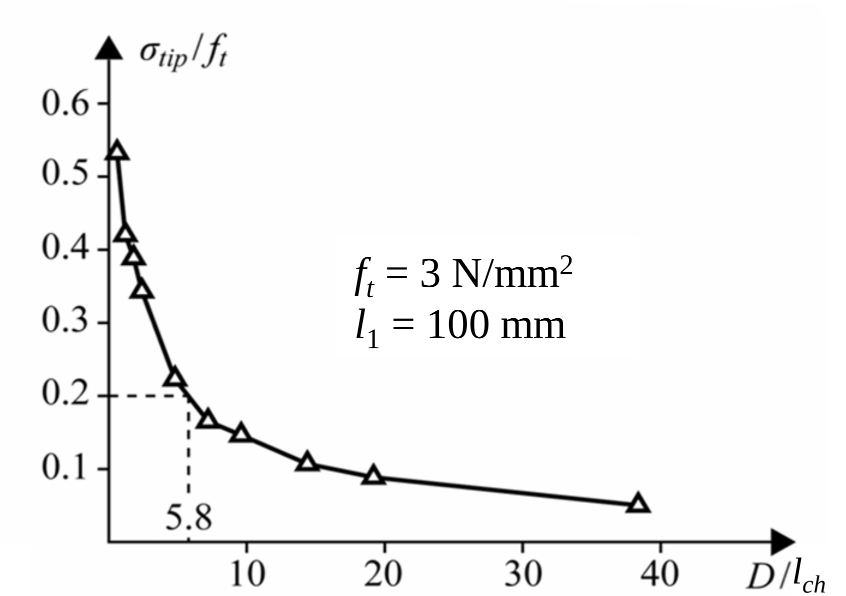

Results for Different Geometries

The numerical calculations were repeated for **single** and **double-notched** traction specimens of the same dimensions

	$l_{FPZ,\infty}$ mm	$l_{FPZ,\infty}/\boldsymbol{l_{ch}}$	c_f mm	$c_f/\boldsymbol{l_{ch}}$	$c_f/l_{FPZ,\infty}$
TPB	68	0.68	38.8	0.388	0.57
SNT	70	0.70	40.7	0.407	0.58
DNT	71	0.71	36.8	0.368	0.52

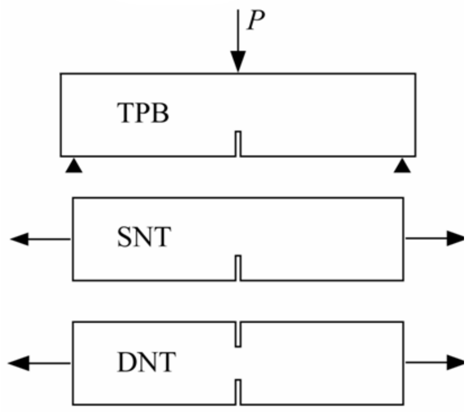

$l_{FPZ,\infty} \cong 0.70 l_{ch}$ $\quad c_f \cong 0.39 l_{ch}$ $\quad c_f \cong 0.55 l_{FPZ,\infty}$

For different geometrical configurations, the values of $\boldsymbol{c_f}$ and $\boldsymbol{l_{FPZ,\infty}}$ are approximately equal.

$f_t = \sqrt{0.39 E G_f / c_f}$ (G_f, c_f from SEL)

$c_f = 0.39 \dfrac{E G_f}{f_t^2}$ (**G_f, f_t from CSEC)**

Experimental investigation

A series of experimental investigations on TPB specimens (Cedolin and Cusatis, 2008) have been conducted at the Politecnico di Milano with the purpose of identifying the **initial portion** of the ***σ*-*w* curve**, with four different concrete compositions.

	Aggregate		Cement		w/c	E	f'_c
	Type	d_a mm	Portland	Quantity kg/m^3		N/mm^2	N/mm^2
N	A	16	325	300	0.60	24200	28.5
S	F	16	525	570	0.44	28600	54.8
B	A	16	325	330	0.55	32680	33.7
C	A	16	325	380	0.50	28690	49.6

Concrete "N"

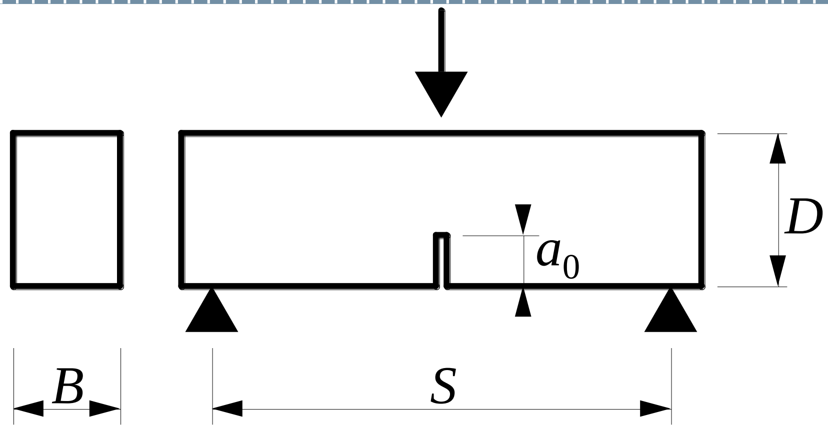

$S/D = 8/3$

$a_0 = 0.3$

notch width = 3 mm

D = 120, 180, 240 mm

B = 80 mm

$\dot{\sigma}_N = 0.012\,\mathrm{N\,mm^{-2}\,sec^{-1}}$

D mm	σ_N N/mm^2	ω (coeff. of variation) %
120	2.07	6.15
180	1.77	7.53
240	1.62	3.35

For **each size**, a series of **3** specimens was tested.

SEL and CCL Identification

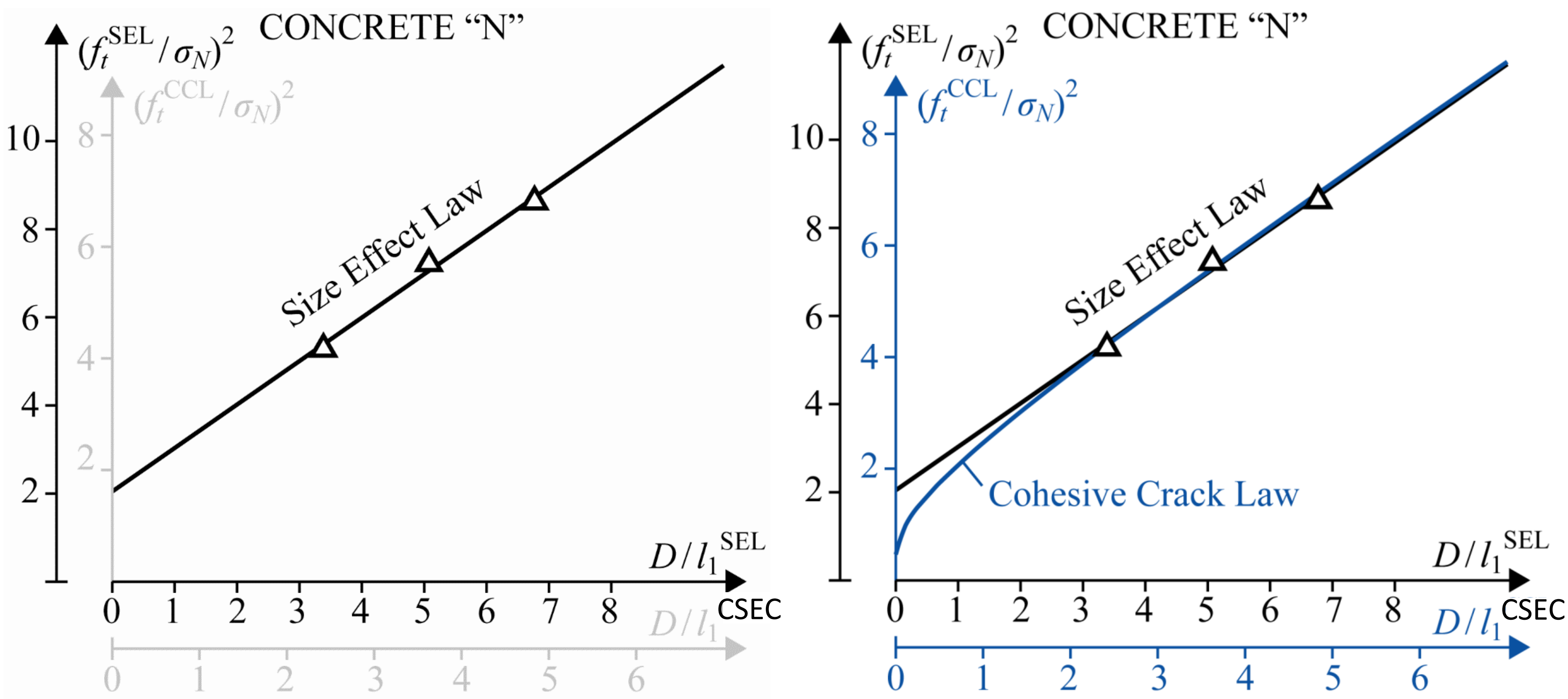

Comparison SEL vs CCL

	G_f N/m	c_f mm	f_t N/mm^2	l_1 mm
SEL	34.5	14.35	4.76 (*)	36.78
CSEC	36.7 (+6%)	18.18 (**) (+27%)	4.23 (–13%)	46.63 (+27%)

$$(*) \quad f_t^{\mathrm{SEL}} = \sqrt{0.39\, E\, G_f^{\mathrm{SEL}} / c_f}$$

$$(**) \quad c_f^{\mathrm{CCL}} = 0.39\, E\, G_f^{\mathrm{CCL}} / f_t^2$$

The difference between the identified values of the initial fracture energy and tensile strength with the two laws (about 6% and 13%) appear to be acceptable. Not so, however, for similar specimens having a different concrete composition (Concrete C, next slide).

Concrete “C”

	G_f N/mm	c_f mm	f_t N/mm^2	l_1 mm
SEL	98.6	53.2	4.55	136
CSEC	152 (+55%)	117 (+120%)	3.07 (–33%)	462 (+240%)

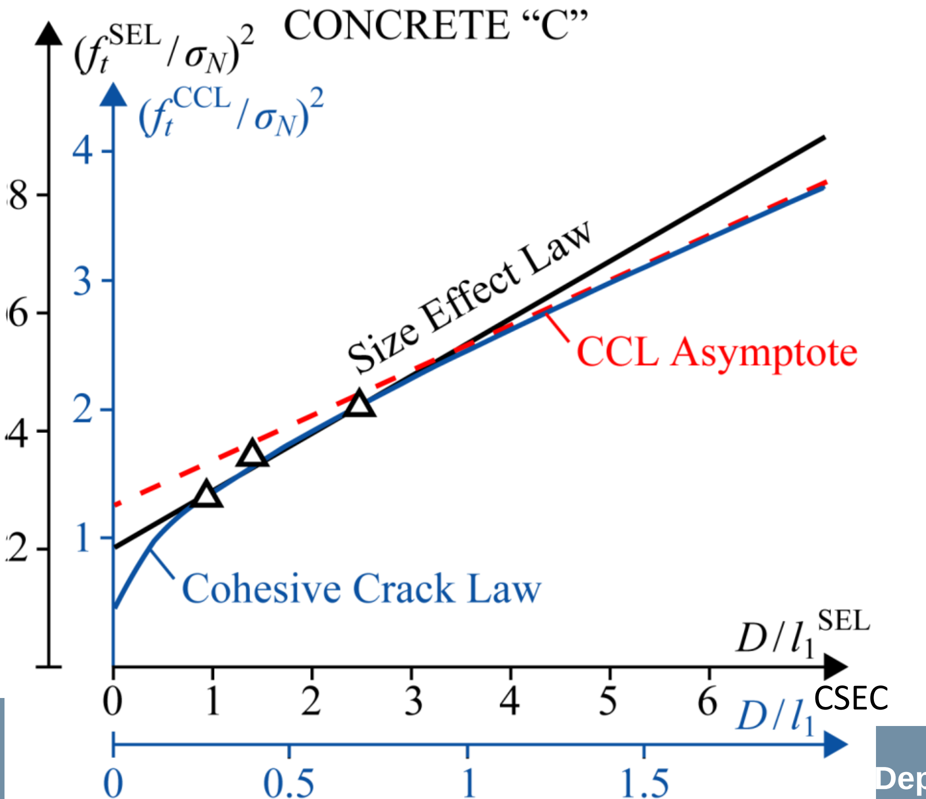

D = 120, 200, and **320 mm**

The specimen sizes give rise to values of ***D/l$_{ch}$*** and of ***X = (g$_0$D)/(g$_0$’ l$_{ch}$)*** which are outside the ranges indicated as valid for the application of the linear softening law by Cedolin and Cusatis (2008) and Cusatis and Schauffert (2009)

Typical FEM Mesh

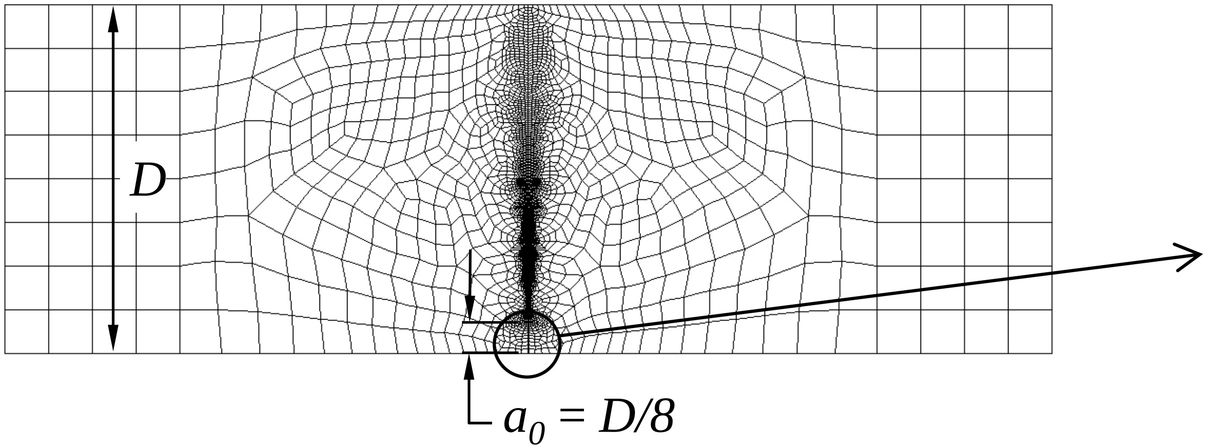

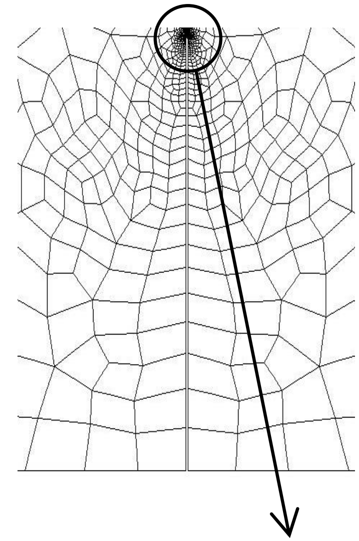

More refined F.E. meshes and much larger values of D/l_{ch} were used by Cusatis and Schauffert (2009)

Cohesive interface elements, with size ≤ 1.0 mm along fracture process zone (FPZ).

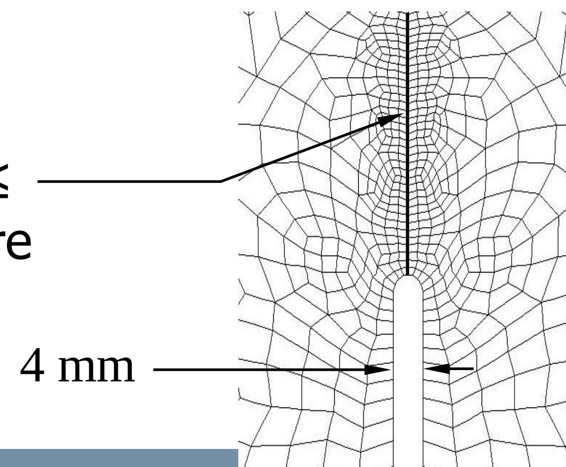

Structural Configurations

a)

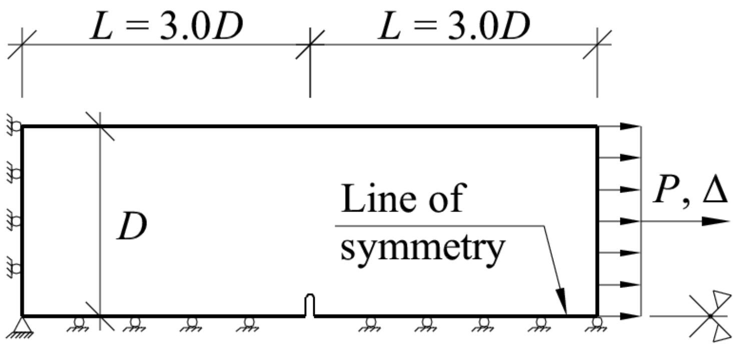

Center Crack Panel (CCP)

b)

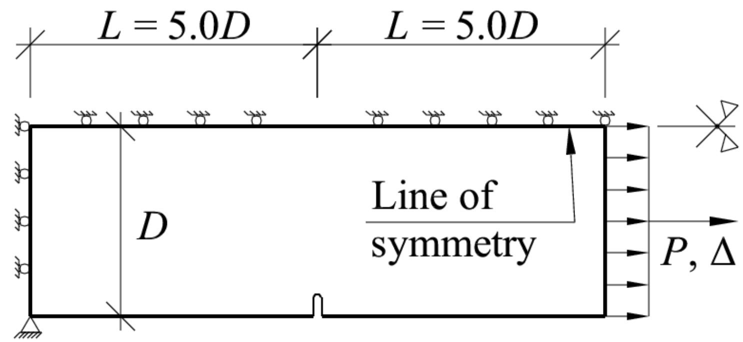

Double Edge Notch Panel (DEN)

c)

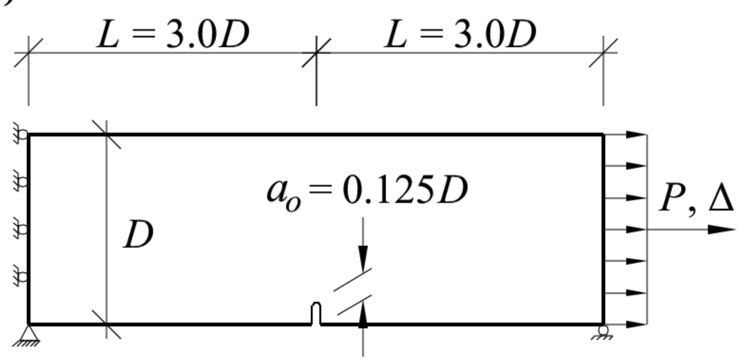

Single Edge Notch Panel (SEN)

d)

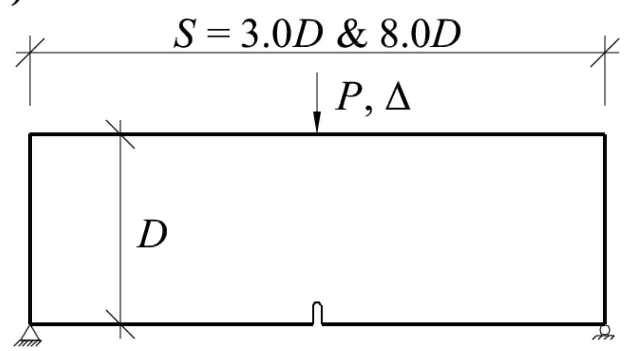

Three Point Bending (TPB3 and TPB8)

CSEC: All Configurations, Linear CCL

- Small size range:

Plastic limits at $D = 0$

distinct size effect behavior

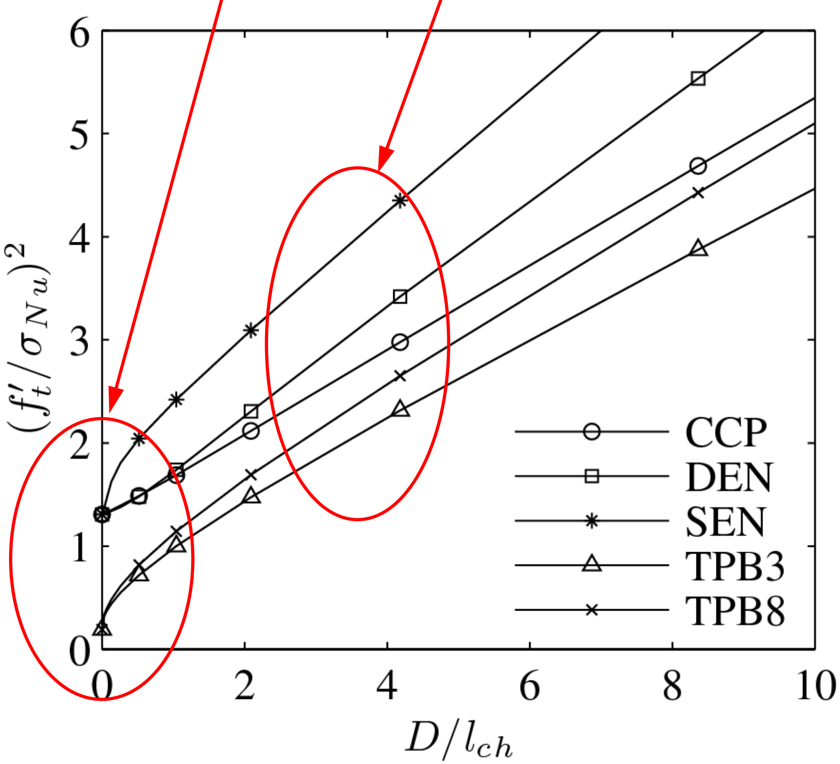

- Large size range:
  - linear correlation coefficients ≈ 1.0;
  - all $\kappa_0 \approx g_0$

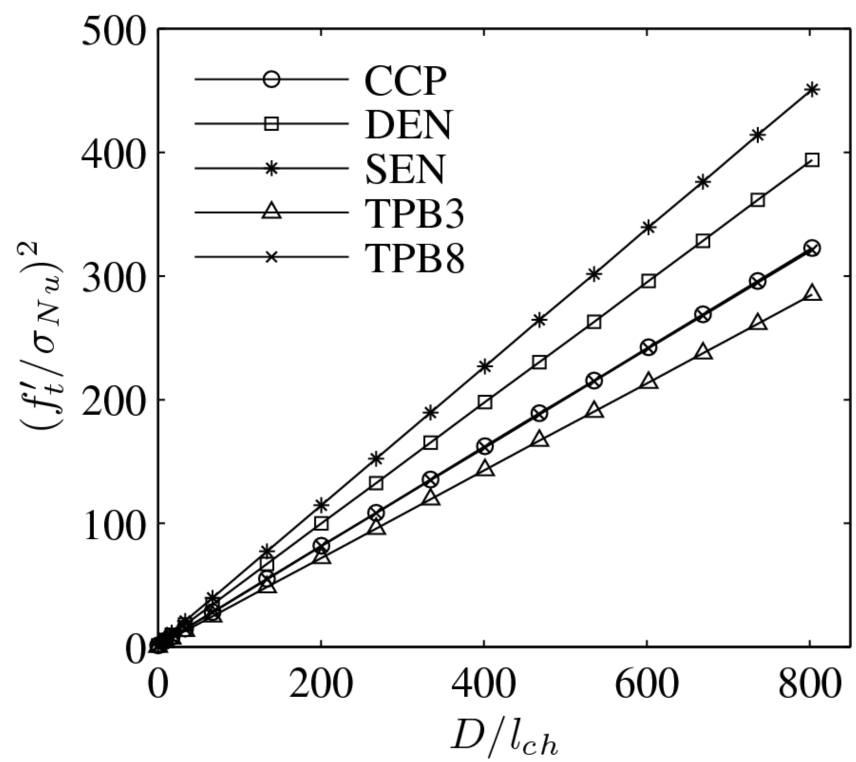

Relation with SEL

- Divide SEL by g_0' :

$$\left(f_t'/\sigma_{nu}\right)^2 \Big/ g_0' = \frac{g_0 D}{g_0' l_{ch}} + \frac{c_F}{l_{ch}}$$

- Plot data as: $X = (g_0 D) \big/ (g_0' l_{ch})$

$$Y = \left(f_t'/\sigma_{nu}\right)^2 \Big/ g_0'$$

Bažant's SEL, linear softening
$c_F = 0.44 l_{CH}$

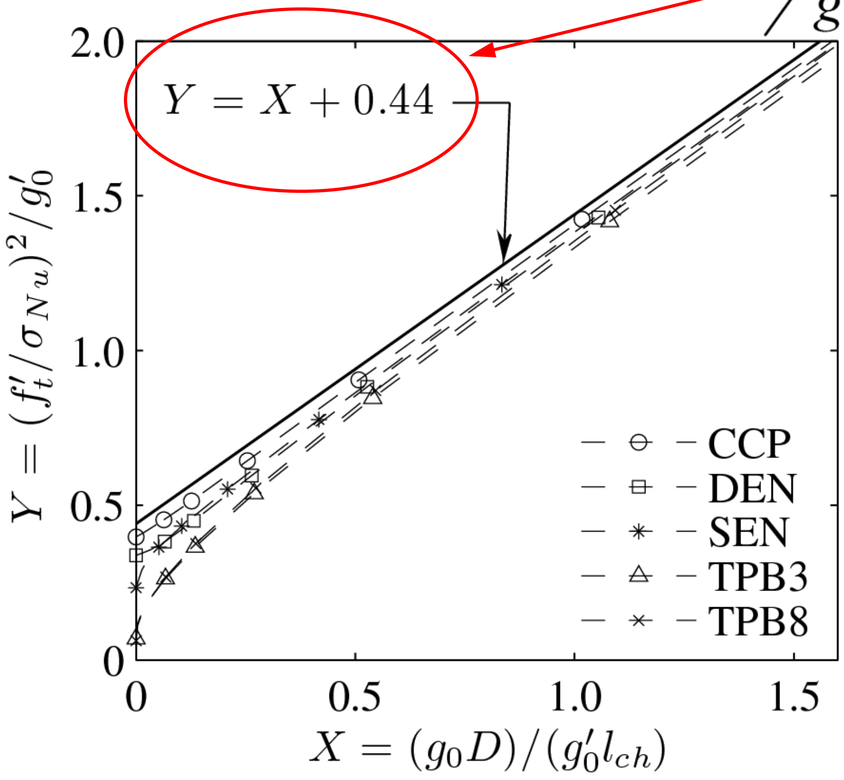

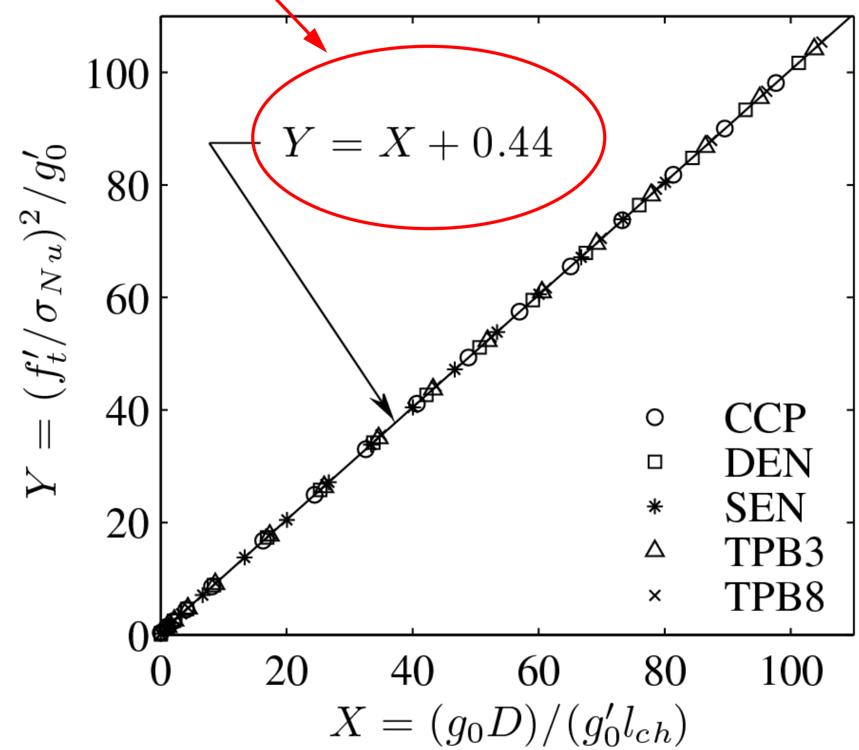

Relation with SEL

- Additional evidence that the common CSEC asymptote represents SEL:
  - length of the FPZ at peak load asymptotically tends to a constant value for all five configurations;
  - cohesive stress at the notch tip tends to zero as size increases.
- Vanishing tip stress and constant FPZ length characterize the analytical derivation of Bažant's SEL.

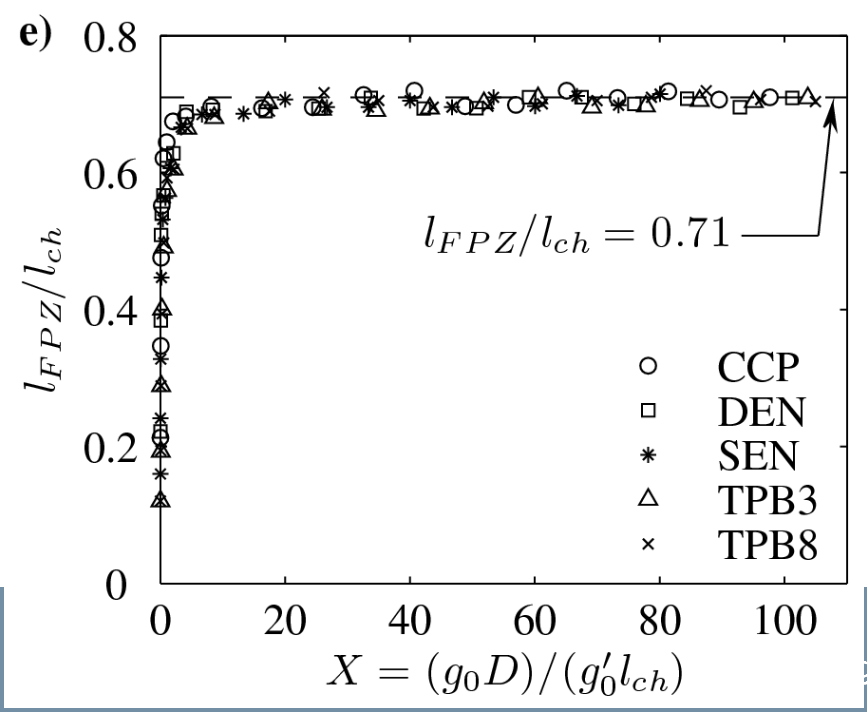

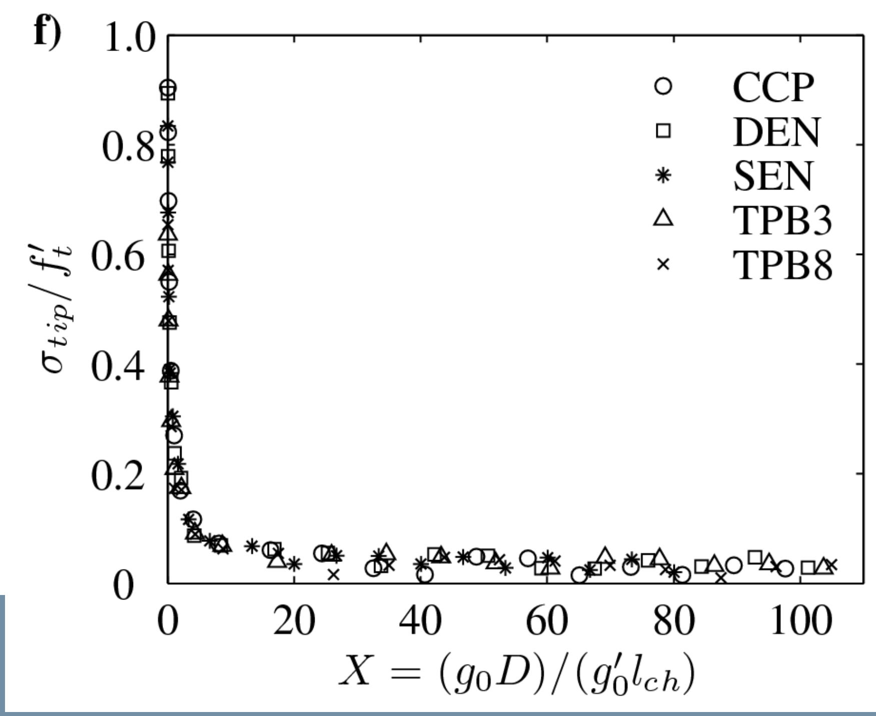

Effective Fracture Process Zone Length

	κ_1	g_0’	c_F / l_{CH}	CV
CCP	1.500	3.288	**0.46**	±5.64%
DEN	1.725	3.871	**0.45**	±6.96%
SEN	2.410	5.603	**0.43**	±6.17%
TPB8	1.445	3.046	**0.47**	±6.78%
TPB3	1.147	2.735	**0.42**	±6.29%

Conclusion: The effective fracture process zone length (EFPZL) relevant to linear softening is independent of structural configuration and has a value of 0.44 ± 0.03.

Bilinear Softening

- Bilinear CCL often assumed for concrete.
- Features chosen to best represent typical concrete:
  - $\gamma = G_F / G_f$ is typically in the range of 1.5 to 2.5. A value of 2.0 was arbitrarily chosen.
  - Reasonable value of $\sigma_{int} = (f'_t / 4)$ was chosen.
- Initial fracture energy, G_f, of the bilinear simulations identical to total fracture energy of the linear softening simulations.

Cusatis and Schauffert (2009) also analyzed the predictions of bilinear softening

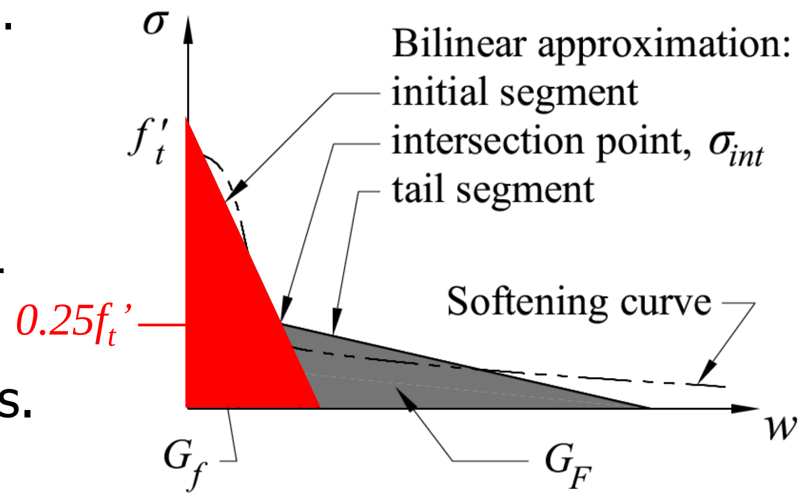

Bilinear Softening

- Bažant's SEL for this particular bilinear CCL: $Y = X + 2.31$
- $c_F = 2.31 l_{ch}$

Difference between SEL-G_f and bilinear CSEC for TPB3 is 20% or less.

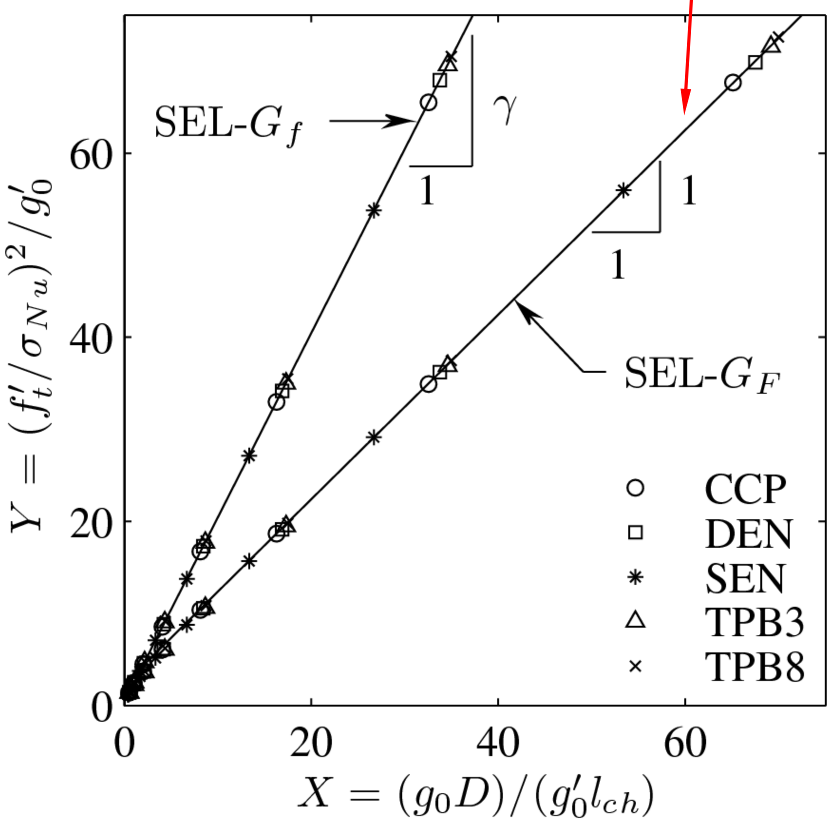

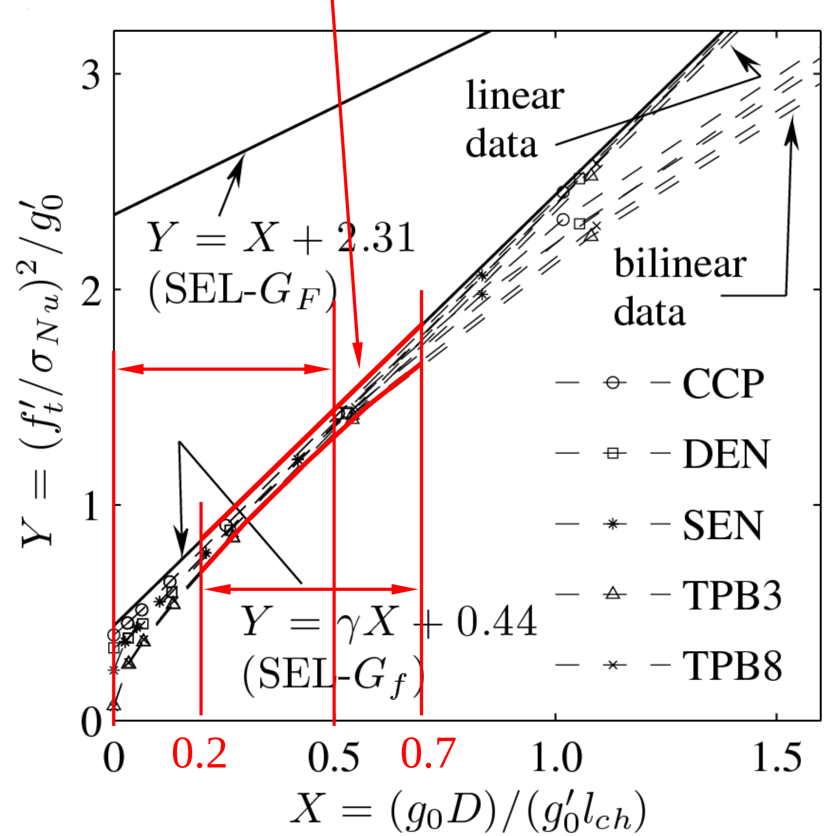

Softening for Small Specimens

True softening of concrete is likely nonlinear, and may feature a region of low slope near the peak.

Characterization of this type of data with a linear softening law can lead to overestimation of initial fracture energy, and possible underestimation of the tensile strength.

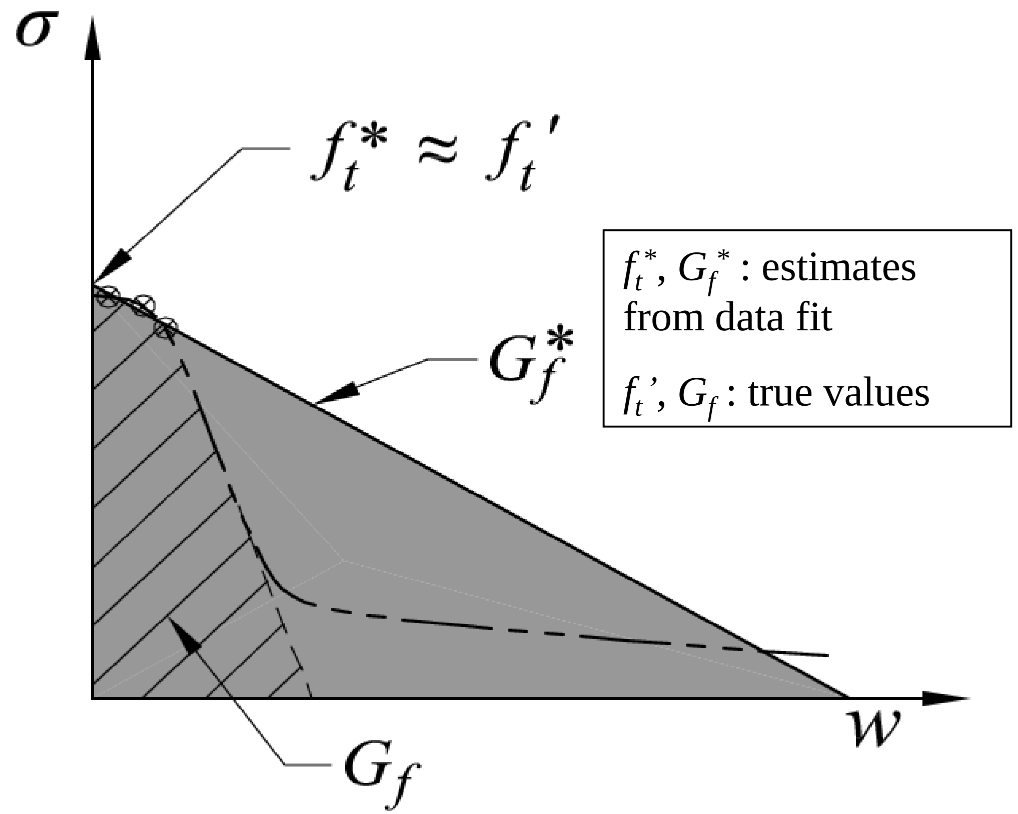

Conclusions

The validity of **Hillerborg's Cohesive Crack Model** for modeling concrete fracture is well-established from all points of view, experimental, theoretical and numerical. This presentation analyzes the results of previous investigations, providing further confirmation. In particular:

- The experimental determination through laser interferometry of the **entire deformation field** (**crack opening included**) along the path of stable crack propagation in tensile test specimens furnishes the capability of **identifying** both the **stress-strain** and the **strain-opening displacement** relations of the Cohesive Crack Model independently of Size Effect Curves.
- The numerical proof that the **asymptotes** of the **CSEC** Curves are defined by parameters which can be considered **material properties** indicates that they must coincide with Bazant's **SEL**, removing in this way any possible conflict and, on the contrary, introducing a relationship between the parameter $\boldsymbol{c_f}$ of **SEL** and the parameter $\boldsymbol{f_t}$ of **CSEC**.

References

The principal references from which many of the figures of this presentation have been taken are:

D.A. Hordijck, *Deformation-controlled uniaxial tensile tests on concrete*, Report 25.5-89-15/VFA, TUDelft, Faculty of Civil Engineering

L. Cedolin, S. Dei Poli, I. Iori, *Tensile behavior of concrete,* ASCE EMJ, Vol. 113, No. 3, March 1987

L. Cedolin, G. Cusatis, *Identification of concrete fracture parameters through size effect experiments*, Cement & Concrete Composites, 2008

G. Cusatis, E.A. Schauffert, *Cohesive crack analysis of size effect*, Engineering Fracture Mechanics 76 (2009) 2163-2173

Personal Remark

In following the developments which led to the understanding of the basic mechanisms involved in concrete fracture, I had the privilege, working on this topic with Zdeňek, of sharing the depth of his thoughts and his passion for scientific truth.

Joining the Framcos Community celebration of his contributions to the establishment of an entirely new theoretical field of nonlinear fracture mechanics, I express my certainty that he will carry on indefinitely on his endevours. ***Best wishes, Zdeňek!***